Journal of Virology

Virology | Full-Length Text

MicroRNA-22-3p displaces critical host factors from the 5′ UTR and inhibits the translation of Coxsackievirus B3 RNA

Priya Rani,[1] Biju George,[1] Sabarishree V,[1] Somarghya Biswas,[1] Madhurya V,[1] Apala Pal,[1] Raju S. Rajmani,[2] Saumitra Das[1,3]

AUTHOR AFFILIATIONS See affiliation list on p. 19.

ABSTRACT Coxsackievirus B3 (CVB3) is known to cause acute myocarditis and pancreatitis in humans. We investigated the microRNAs (miRNAs) that can potentially govern the viral life cycle by binding to the untranslated regions (UTRs) of CVB3 RNA. MicroRNA-22-3p was short-listed, as its potential binding site overlapped with the region crucial for recruiting internal ribosome entry site *trans*-acting factors (ITAFs) and ribosomes. We demonstrate that miR-22-3p binds CVB3 5′ UTR, hinders recruitment of key ITAFs on viral mRNA, disrupts the spatial structure required for ribosome recruitment, and ultimately blocks translation. Likewise, cells lacking miR-22-3p exhibited heightened CVB3 infection compared to wild type, confirming its role in controlling infection. Interestingly, miR-22-3p level was found to be increased at 4 hours post-infection, potentially due to the accumulation of viral 2A protease in the early phase of infection. $2A^{pro}$ enhances the miR-22-3p level to dislodge the ITAFs from the SD-like sequence, rendering the viral RNA accessible for binding of replication factors to switch to replication. Furthermore, one of the cellular targets of miR-22-3p, protocadherin-1 (PCDH1), was significantly downregulated during CVB3 infection. Partial silencing of PCDH1 reduced viral replication, demonstrating its proviral role. Interestingly, upon CVB3 infection in mice, miR-22-3p level was found to be downregulated only in the small intestine, the primary target organ, indicating its possible role in influencing tissue tropism. It appears miR-22-3p plays a dual role during infection by binding viral RNA to aid its life cycle as a viral strategy and by targeting a proviral protein to restrict viral replication as a host response.

IMPORTANCE CVB3 infection is associated with the development of end-stage heart diseases. Lack of effective anti-viral treatments and vaccines for CVB3 necessitates comprehensive understanding of the molecular players during CVB3 infection. miRNAs have emerged as promising targets for anti-viral strategies. Here, we demonstrate that miR-22-3p binds to 5′ UTR and inhibits viral RNA translation at the later stage of infection to promote viral RNA replication. Conversely, as host response, it targets PCDH1, a proviral factor, to discourage viral propagation. miR-22-3p also influences CVB3 tissue tropism. Deciphering the multifaced role of miR-22-3p during CVB3 infection unravels the necessary molecular insights, which can be exploited for novel intervening strategies to curb infection and restrict viral pathogenesis.

KEYWORDS Coxsackievirus B3, microRNAs, IRES-mediated translation

Coxsackievirus B3 (CVB3) is a positive-strand RNA virus from the Picornaviridae family that spreads through the fecal-oral route. It is a human pathogen infecting the heart, pancreas, and brain causing myocarditis, acute pancreatitis, and aseptic meningitis, respectively. The inflammation caused by viral infection leads to long-term fatal diseases such as dilated cardiomyopathy and type I diabetes. To establish infection, CVB3

Editor Christiane E. Wobus, University of Michigan Medical School, Ann Arbor, Michigan, USA

Address correspondence to Saumitra Das, sdas@iisc.ac.in.

The authors declare no conflict of interest.

See the funding table on p. 20.

Received 25 September 2023
Accepted 2 January 2024
Published 30 January 2024

is completely dependent on the host machinery, and the host factors such as proteins and non-coding RNAs play a major role in it (1–4).

Among the non-coding RNAs, microRNAs (miRNAs) have been implicated in influencing CVB3 life cycle in many ways. miRNAs can exert both direct and indirect effects during viral infections (5). The indirect mechanism involves their control over viral replication by targeting specific genes within the host genome. In CVB3 infection, miRNAs play critical roles in regulating viral replication and host responses. Upregulated miRNAs like miR-203 enhance viral replication and cell survival by targeting ZFP-148 (6). Additionally, miR-590-5p in vesicles from infected cells prolongs viral replication by targeting SPRY1 (7). miR-126 upregulation modulates the ERK1/ERK2 and Wnt/b-catenin pathways, promoting virus replication and release (8). Conversely, miR-221/miR-222 suppress target genes to limit viral replication and inflammation, protecting the heart during CVB3 infection (9). Moreover, during CVB3 infection, the virus carefully manipulates cell apoptosis to facilitate its replication and spread. Specific miRNAs, such as miR-34a, miR-222, miR-98, and miR-21, play crucial roles in regulating this process. miR-34a acts as a proapoptotic factor, while miR-222, miR-98, and miR-21 act as anti-apoptotic factors in viral myocarditis (VMC) (10–14).

There are a few reports suggesting the direct involvement of miRNAs during CVB3 infection. Bioinformatic analysis has revealed that miR-342-5p potentially targets the 2C-coding region of the CVB3 viral genome, effectively inhibiting viral replication by directly acting on this region. Interestingly, not all miRNAs function as negative regulators (15). Another miRNA, miR-10a*, plays a unique role in promoting viral biosynthesis by targeting the 3D-coding region (nt6818–nt6941) of CVB3. Furthermore, miR-10a* is found to be abundant in the heart of BALB/c mice, suggesting its potential influence on VMC by enhancing CVB3 replication (16). However, there are reports of miRNAs exhibiting anti-viral effects by targeting viral RNA and inducing gene silencing. Highly conserved miRNA-binding sites in RNA viruses may be utilized by viruses to evade immunity, prolong incubation periods, or increase virulence. Examples include Eastern equine encephalitis virus, where miR-142-3p-binding sites enhance neurovirulence, and human immunodeficiency virus type 1, where miRNAs inhibit viral production by targeting RNA and host proteins (17, 18). In the case of chikungunya virus (CHIKV), *Aedes aegypti* miR-2944b-5p binds to CHIKV 3′ untranslated region (UTR), reducing CHIKV replication and regulating cellular targets, contributing to virus survival and transmission (19). Another example includes miR-122 interacting with the 5′ UTR of hepatitis C virus (HCV) RNA, forming a trimolecular RNA structure crucial for efficient virus proliferation. miR-122 protects uncapped HCV RNA from degradation and stabilizes viral RNA, altering its secondary structure and influencing HCV proliferation (20–22). Similarly, endogenous miR-548g-3p suppresses dengue virus (DENV) replication by binding to the conserved stem-loop promoter (SLA) in the 5′ UTR, potentially disrupting the natural SL structure and affecting DENV promoter efficiency (23). These findings indicate the potential utility of miRNAs as a valuable treatment approach to directly impede viral replication by specifically targeting crucial regions of the viral genome.

The direct influence of miRNAs on the CVB3 life cycle piqued our interest, considering the high likelihood of viral RNA being targeted by host miRNAs. Consequently, our focus shifted toward identifying miRNAs that may exhibit binding affinity toward the UTRs of the viral RNA, as UTRs play an essential role in viral RNA translation and replication. We were interested to explore if miRNAs with possible binding to the UTRs may have an impact on CVB3 life cycle.

RESULTS

miR-22-3p levels are induced upon CVB3 infection and it binds to the 5′ UTR of CVB3 RNA

Using the VITA database (24), we successfully obtained a list of miRNAs with a strong binding probability to both the 5′ and 3′ UTRs of CVB3. Notably, one of the miRNAs, miR-22-3p, had a predicted binding site within the 5′ UTR, precisely between stem loop

V and VI (Fig. 1A). The prediction was further confirmed by another software, STarMir (Fig. 1B) (25–27). The region between stem loop V and VI is a crucial region in the CVB3 5′ UTR, as it is known to facilitate interactions with several host RNA-binding proteins, subsequently promoting CVB3 RNA translation (28, 29). Additionally, this region contains a Shine-Dalgarno-like sequence, which serves as the recruitment site for the ribosomal small subunit to start scanning, leading to translation initiation at the initiator AUG codon (30).

miR-22-3p is a well-studied miRNA with diverse roles in various disease conditions. In the context of cancer, it acts as a tumor suppressor (31–34), while in arthritis, it exhibits anti-inflammatory properties (35). Downregulation of miR-22-3p levels has been observed in Alzheimer's disease, contributing to protein aggregate formation and disease progression (36, 37). Of particular interest, miR-22-3p has also been implicated in several cardiac pathologies. It is abundantly expressed in the heart, and studies have revealed that when miR-22-3p is knocked out in mice hearts and cardiac stress is given to the mice, it results in the development of cardiac dilation and fibrosis, a phenotype similar to the pathogenesis induced by CVB3 infection. Moreover, miR-22-3p levels are increased during cardiac hypertrophy, highlighting its crucial role in the cardiac remodeling process (38, 39). Given the intriguing properties of miR-22-3p, we further explored its potential role during CVB3 infection.

Our primary interest was to investigate the expression level of miR-22-3p during CVB3 infection, speculating that a miRNA that is upregulated had a higher chance of binding to CVB3 RNA and influencing its functions. We employed two distinct model systems to investigate miR-22-3p expression post-CVB3 infection: HeLa cells, a well-established cell culture model to study CVB3 life cycle and male BALB/c mice (3–4 weeks old) as an *in vivo* model system. We performed quantitative PCR (qPCR) to analyze miR-22-3p expression using total RNA extracted from CVB3-infected HeLa cells and the heart tissues of mice. Our findings revealed an upregulation of miR-22-3p in HeLa cells 8 hours post-infection (h.p.i.), and a similar induction was observed in the heart tissues of CVB-infected mice 7 days post-infection (d.p.i.). Additionally, we included miR-21–5p, a known upregulated miRNA upon CVB3 infection, as a positive control in our study (Fig. 1C).

Given that miR-22-3p exhibited upregulation during CVB3 infection and was predicted to have a binding site in the CVB3 5′ UTR, our initial goal was to validate this binding between miR-22-3p and CVB3 RNA. To accomplish this, we introduced a miR-22-3p binding mutation into the CVB3 5′ UTR as depicted in Fig. 1D. Next, the mutant and wild-type (WT) 5′ UTR were tagged to MS2 RNA. Subsequently, a tagged RNA affinity pull-down (TRAP) assay was conducted to assess the presence of miR-22-3p through pull-down. The results, as clearly observed in Fig. 1E, demonstrated that the pull-down fraction of the WT CVB3 5′ UTR exhibited enrichment of miR-22-3p, while the mutant CVB3 5′ UTR with impaired miR-22-3p binding did not show this enrichment. We further corroborated this binding by conducting pull-down experiments using the Ago-2 antibody following miR-22-3p overexpression, leading to the detection of a higher amount of CVB3 RNA in the pull-down fraction (Fig. 1F). These observations provide compelling evidence that miR-22-3p indeed binds to the predicted site in the 5′ UTR of CVB3 RNA.

miR-22-3p negatively regulates CVB3 life cycle

Our subsequent focus was on investigating the regulatory role of miR-22-3p binding in the CVB3 life cycle. To delve into this aspect, we employed a CVB3 replicon construct (Fig. 2A) where the CVB3 structural genes were replaced with the Firefly luciferase gene. This replicon serves as a non-infective, replicating CVB3 genome. In our experimental setup, we either overexpressed miR-22-3p or carried out partial silencing of miR-22-3p in HeLa cells, which were then transfected with the CVB3 replicon RNA. Cells were harvested 8 hours post-transfection, and luciferase activity was measured. We observed an almost 50% reduction in luciferase activity when miR-22-3p was overexpressed. Conversely, when miR-22-3p was partially knocked down, the luciferase activity increased by 1.5-fold,

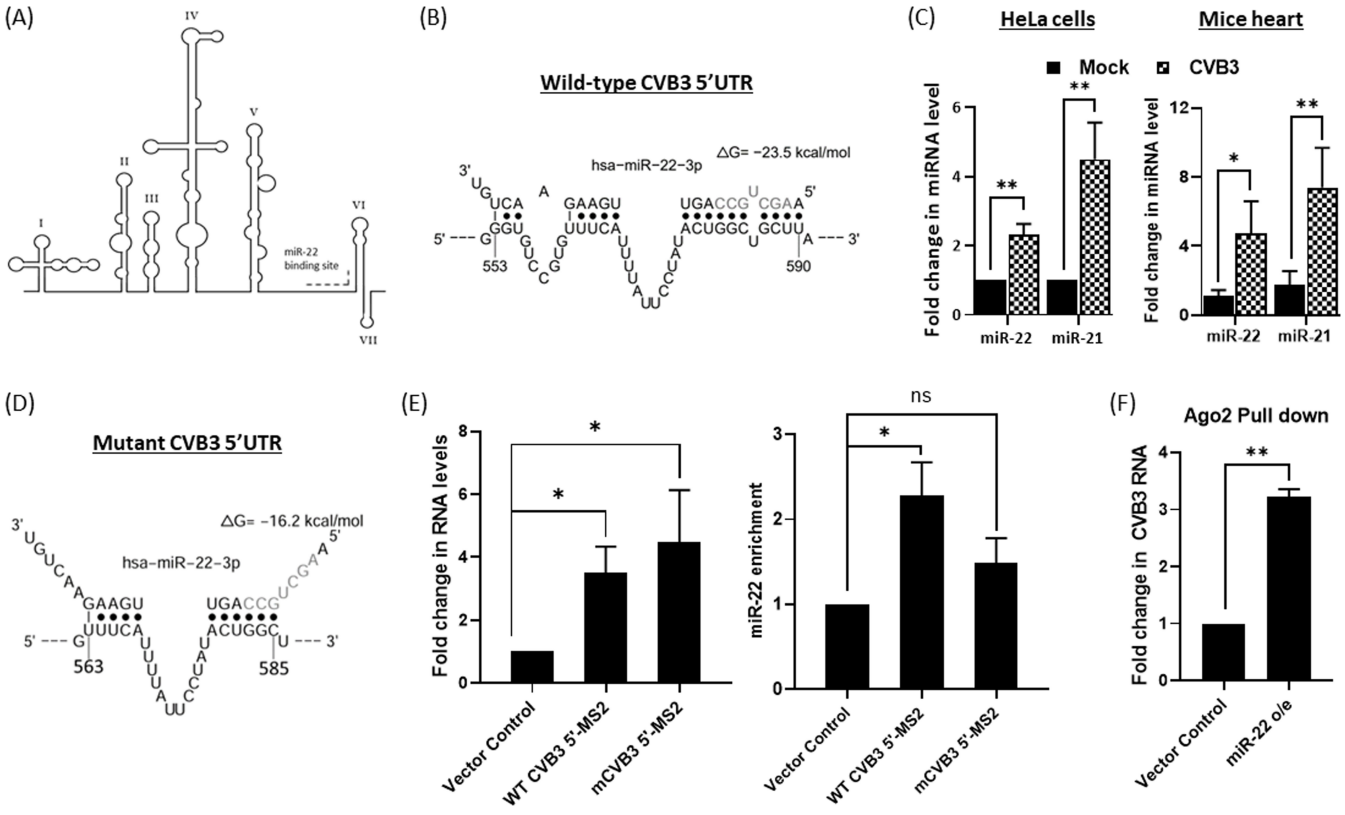

FIG 1 miR-22-3p levels are induced upon CVB3 infection, and it binds to the 5′ UTR of CVB3 RNA. (A) Schematic representation of predicted miR-22-3p binding site in the CVB3 5′ UTR. (B) The schematic represents the complementarity between miR-22-3p and CVB3 sequences. The sequence in gray is the seed sequence of miR-22-3p. The schematic is generated through STarMir. (C) HeLa cells were seeded at a confluency of 90% and infected with CVB3 (multiplicity of infection 10). Cells were harvested at 8 hours post-infection, and total RNA was isolated from the lysate. miR-22-3p and miR-21-5p levels were checked using quantitative PCR (qPCR). Error bars represent standard deviation in three independent experiments (left panel). Three- to four-week-old male BALB/c mice were injected with 10^4 PFU of CVB3 intraperitoneally. Seven days post-infection, the animals were sacrificed, and the mice hearts were harvested. Total RNA was isolated from the tissues, and miR-22-3p and miR-21-5p levels were checked using qPCR. Error bars represent standard deviations in five biological replicates (right panel). (D) Schematic representation of miR-22-3p binding mutation in the CVB3 5′ UTR (generated by STarMir). The sequence in gray is the seed sequence of miR-22-3p. (E) CVB3 5′ UTR [wild type (WT) or miR-22-3p binding defective] overexpression construct and pMS2-GST constructs were co-transfected in HeLa cells. The bar graph on the left shows the level of overexpression of the CVB3 5′ UTR constructs. The bar graph on the right shows the miR-22-3p enrichment in the pull-down fractions using qPCR. (F) HeLa cells were transfected with either pSUPER (vector control) or miR-22-3p overexpression construct, and pull-down was done using Ago-2 antibody from the cellular extract harvested 8 hours post-transfection. The bar graph represents the qPCR analysis of CVB3 RNA present in the miR-22-3p overexpression cells as compared to the vector control. The RNA was normalized with the input CVB3 RNA present in the extract. Error bars represent standard deviations in three independent experiments. *$P < 0.05$, **$P < 0.01$. ns, not significant.

as illustrated in Fig. 2B. To further substantiate these findings, we conducted experiments using a CVB3 replicon with a mutation that impairs its binding to miR-22-3p (same mutation as was used for TRAP assay). We observed that while miR-22-3p overexpression decreased the luciferase activity of the WT CVB3 replicon, the mutant replicon showed no such effect, as shown in Fig. 2C. These collective results strongly suggest that miR-22-3p exerts a negative regulatory influence on the CVB3 life cycle.

Our curiosity led us to probe the specific stage in the CVB3 life cycle where miR-22-3p exerts its influence. To address this, we investigated the impact of miR-22-3p on CVB3 RNA translation by utilizing guanidine hydrochloride (GuHCl), a replication-inhibiting drug. In the experiment, HeLa cells were transfected with CVB3 replicon RNA, in the context of either overexpression of miR-22-3p or partial silencing. These transfections were conducted in the presence or absence of 2-mM GuHCl. Surprisingly, we found that miR-22-3p still exhibited its inhibitory effect on the luciferase activity of the CVB3 replicon, even when GuHCl was present (Fig. 2D). To further validate the specificity of

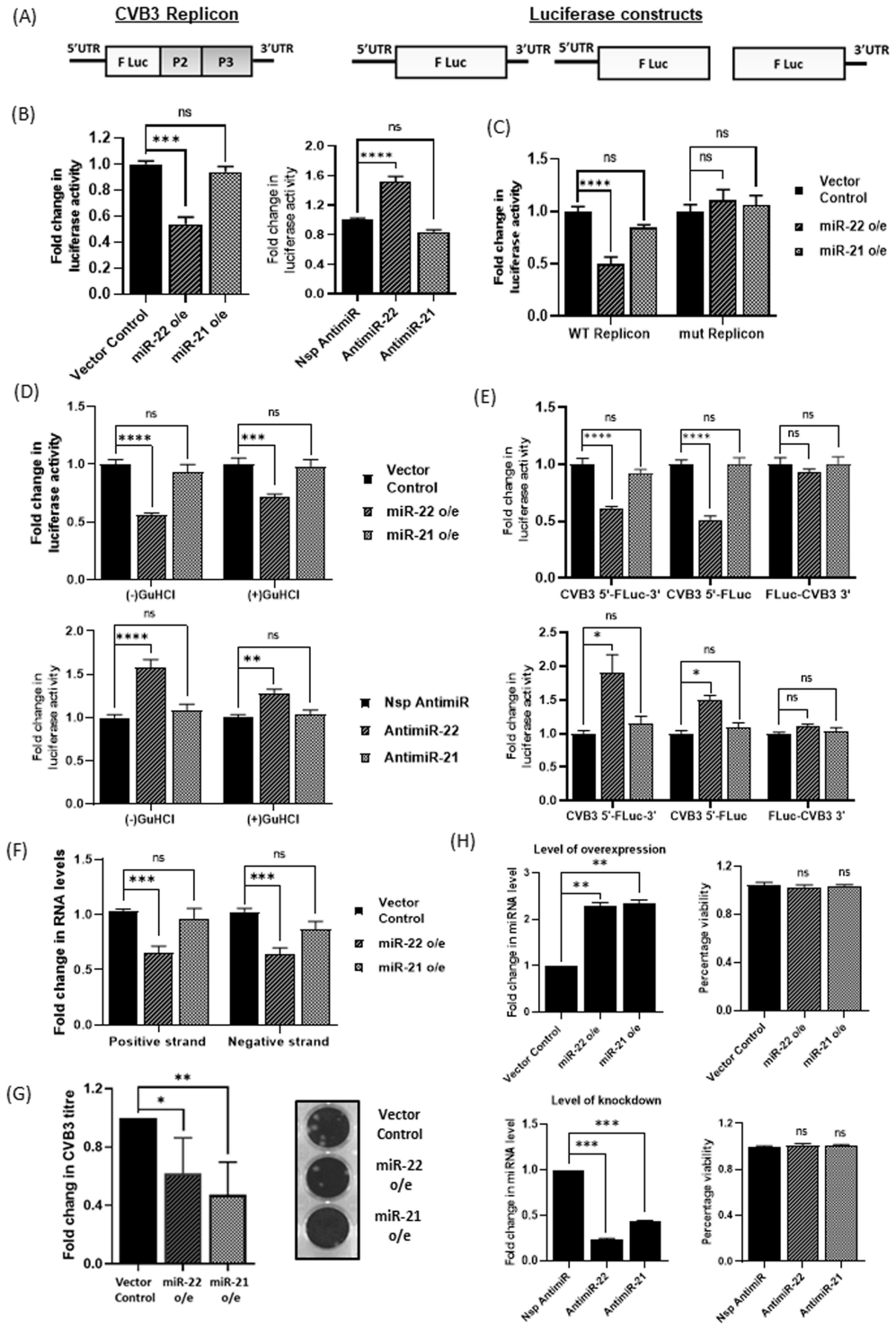

FIG 2 miR-22-3p negatively regulated CVB3 life cycle. (A) Schematic representation of the luciferase constructs used in the experiments. (B) HeLa cells were transfected with pSUPER (vector control), miR-22-3p, or miR-21-5p overexpression plasmids for overexpression experiment and non-specific anti-miRNA, anti-miR-22-3p, or anti-miR-21-5p for partial knockdown experiment. After 24 hours, CVB3 replicon RNA was transfected, and the cells were harvested after 8 hours followed by checking of the luciferase activity. The bar graph on the left represents the fold change in luciferase activity of CVB3 replicon upon miR-22-3p or miR-21–5p overexpression. The bar graph on the right represents the fold change in luciferase activity of CVB3 replicon upon partial knockdown of miR-22-3p or miR-21-5p. (C) HeLa cells with miR-22-3p overexpressed were transfected with either WT or miR-22-3p binding defective CVB3 replicon RNA and harvested after 8 hours. Fold change

(Continued on next page)

FIG 2 (Continued)

in luciferase activity is represented as the bar graph. (D) HeLa cells overexpressing vector control, miR-22-3p, or miR-21-5p were transfected with CVB3 replicon RNA either in the absence or in the presence of 2-mM GuHCl in media. Cells were harvested 8 hours post-transfection, and luciferase activity was measured (upper panel). HeLa cells transfected with Nsp anti-miR, anti-miR-22-3p, or anti-miR-21-5p were further transfected with CVB3 replicon RNA either in the absence or in the presence of 2-mM GuHCl in media. Cells were harvested 8 hours post-transfection, and luciferase activity was measured (bottom panel). (E) HeLa cells overexpressing vector control, miR-22-3p, or miR-21-5p were transfected with each of the described luciferase construct RNAs. Cells were harvested 8 hours post-transfection, and luciferase activity was measured. The bar graph represents the fold change in luciferase activity (upper panel). HeLa cells transfected with Nsp anti-miR, anti-miR-22-3p, or anti-miR-21-5p were further transfected with each of the described luciferase construct RNAs. Cells were harvested 8 hours post-transfection, and luciferase activity was measured. The bar graph represents the fold change in luciferase activity (bottom panel). (F) HeLa cells overexpressing vector control, miR-22-3p, or miR-21-5p were infected with CVB3 at an multiplicity of infection (MOI) of 10. Cells were harvested at 8 h.p.i., and total RNA was isolated from the cell. CVB3 RNA was quantified by qPCR. The bar graph represents the fold change in the positive and negative strands of CVB3 RNA. (G) HeLa cells overexpressing vector control, miR-22-3p, or miR-21-5p were infected with CVB3 at an MOI of 10. Supernatant was collected at 8 h.p.i.and was used to perform plaque assay. The bar graph represents the fold change in the virus titer. (H) HeLa cells were transfected with either vector control, miR-22-3p, or miR-21-5p overexpression plasmids, or with Nsp anti-miR, anti-miR-22-3p, or anti-miR-21-5p; 24 hours post-transfection, 3-(4,5-dimethylthiazol-2-yl)−2,5-diphenyltetrazolium bromide reagent was added to the wells, and after 3–4 hours, Dulbecco's Modified Eagle Medium (DMEM) was removed, and Dimethyl sulfoxide (DMSO) was added and mixed well. Reading was taken at 550 nm in a spectrophotometer. One well from each condition was kept for checking the level of overexpression of the miRNAs. The bar graphs on the left show the level of overexpression or knockdown, and bar graphs on the right show viability in percentage. Error bars represent standard deviations in three independent experiments. *$P < 0.05$, **$P < 0.01$, ***$P < 0.001$, ****$P < 0.0001$.

the observed effect, we performed an additional assay using three different luciferase constructs: CVB3 5′ UTR-FLuc-CVB3 3′ UTR, CVB3 5′ UTR-FLuc, and FLuc-CVB3 3′ UTR (Fig. 2A). Results showed that miR-22-3p only affected the luciferase activity of the constructs containing the CVB3 5′ UTR, as shown in Fig. 2E. Taken together, these results indicate that miR-22-3p binding to the CVB3 5′ UTR exerts a negative impact on CVB3 RNA translation.

We aimed to extend our findings beyond the CVB3 replicon and luciferase construct experiments to confirm if the observed effects are reproducible in the context of CVB3 infection. To accomplish this, we overexpressed miR-22-3p in HeLa cells and infected them with CVB3 at a multiplicity of infection (MOI) of 10, followed by harvesting the cells 8 h.p.i. We isolated total RNA from the cell lysate and collected the supernatant for plaque assays. Our results indicated that both the positive and negative strand CVB3 RNA levels were notably reduced in the cells overexpressing miR-22-3p, as depicted in Fig. 2F. Additionally, the viral titer of CVB3 produced by these cells was diminished by 40% (Fig. 2G). We performed 3-(4,5-dimethylthiazol-2-yl)−2,5-diphenyltetrazolium bromide (MTT) assays to ensure that the alteration of miR-22-3p expression itself did not adversely impact the cells, as shown in Fig. 2H. Thus, it appears that miR-22-3p acts as a negative regulator of the CVB3 infection cycle.

CVB3 proliferation is increased in miR-22-3p knockout cells

To reconfirm our findings, we established a miR-22-3p knockout (KO) cell line. The KO was verified through sequencing (data not shown) and quantitative PCR analysis, as illustrated in Fig. 3A. CVB3 infection (MOI 10) was carried out in both the WT and miR-22-3p KO HeLa cells, which were seeded at 90% confluency. After 8 h.p.i., we examined the results. Interestingly, in the miR-22-3p KO cells, we observed significant upregulation of both the CVB3 positive and negative RNA strands compared to the WT HeLa cells (Fig. 3B), confirming the trends seen in our earlier experiments. Furthermore, the virus titer produced from the miR-22-3p KO cells was found to be approximately threefold higher, providing additional evidence for the role of miR-22-3p as an anti-viral factor during CVB3 infection (Fig. 3C).

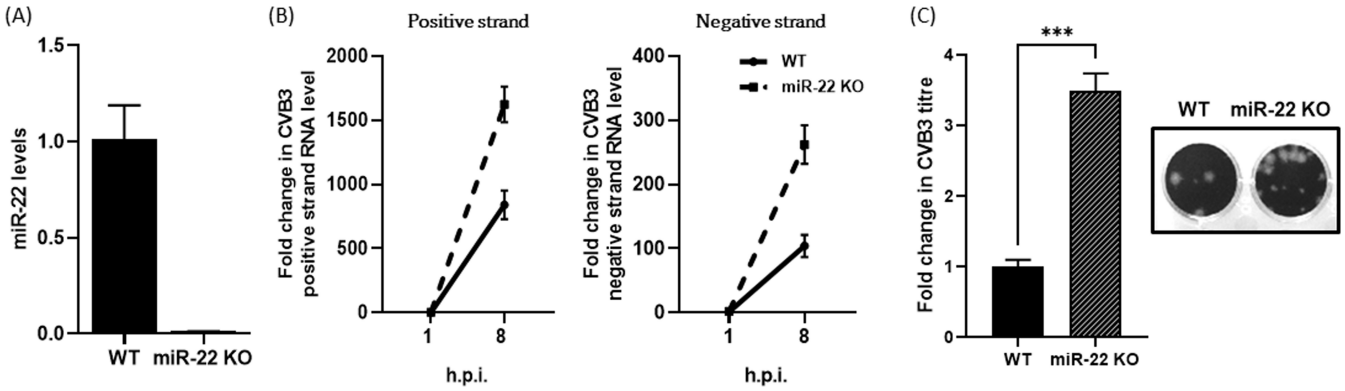

FIG 3 CVB3 proliferation is enhanced in miR-22-3p KO cells. (A) Total RNA was isolated from WT HeLa and miR-22-3p KO HeLa cells, and miR-22-3p levels were detected by qPCR. The bar graph represents the fold change in miR-22-3p levels. (B) WT and miR-22-3p KO cells seeded at 90% confluency were infected with CVB3 (MOI 10) and harvested at 1 hour and 8 h.p.i.. Total RNA was isolated and CVB3 positive and negative RNA strands were quantified by qPCR. The line graphs represent the fold change in the level of CVB3 RNA in miR-22-3p KO cells with respect to WT cells. (C) WT and miR-22-3p KO cells seeded at 90% confluency were infected with CVB3 (MOI 10), and the supernatant was collected at 8 h.p.i. to perform plaque assay. The bar graph represents the fold change in the virus titer. Error bars represent standard deviations in three independent experiments. *$P < 0.05$, **$P < 0.01$, ***$P < 0.001$, ****$P < 0.0001$.

MicroRNA-22 binding reduces the binding of translation-promoting ITAFs

Having established the role of miR-22-3p in CVB3 infection, we aimed to decipher the mechanisms underlying its effects. As previously mentioned, the site where miR-22-3p binds also serves as a binding site for several internal ribosome entry site *trans*-acting factors (ITAFs) known to enhance CVB3 translation, specifically, La, PSF, and PTB (Fig. 4A). We were particularly interested in understanding how miR-22-3p binding influenced the interaction between these ITAFs and the CVB3 5′ UTR. To investigate this, we conducted immunoprecipitation experiments after infecting HeLa cells transfected with vector control or miR-22-3p overexpression plasmid, with CVB3. miR-22-3p overexpression in the cell lysate (input fraction) was confirmed by qPCR (data not shown). Antibodies specific to each of the ITAFs were used, and we assessed the association between CVB3 RNA and these ITAFs under both conditions. As a negative control for our experiment, we utilized the HuR protein, another RNA-binding protein that harbors a binding site in a different stem loop of the CVB3 5′ UTR (40). Interestingly, our findings revealed a reduced association of CVB3 RNA with La, PSF, and PTB upon miR-22-3p overexpression (Fig. 4B through D). However, there was no discernible effect on the association of CVB3 RNA with the HuR protein (Fig. 4E). These results suggest that miR-22-3p displaces the binding of some ITAFs to the CVB3 5′ UTR, specifically between stem loops V and VI.

MicroRNA-22 binding inhibits translation by inhibiting ribosome recruitment

One of the ITAFs that was displaced due to miR-22-3p binding to the CVB3 5′ UTR was the La protein. Earlier, we have demonstrated the crucial role of La binding in facilitating ribosome recruitment to the CVB3 5′ UTR (30). Therefore, we were curious to examine whether miR-22-3p binding was also influencing ribosome recruitment. To address this question, we employed the polysome profiling technique. We evaluated the level of CVB3 RNA associated with the 40S ribosomal subunit, complete monosomes, and polysomes in cells with and without miR-22-3p. Initially, we assessed whether there were any differences in the polysome profiles between WT and miR-22-3p KO HeLa cells. As illustrated in Fig. 5A, the profiles were nearly identical. Subsequently, we infected the cells with CVB3 and performed polysome profiling on the lysates from the infected cells. Upon infection, a drastic decrease in the polysomes was observed, because CVB3 infection shuts off global translation (Fig. 5B). We separately isolated RNA from the 40S fraction, the monosomes, and the polysomes. As anticipated, we found that CVB3 RNA was more abundant in all fractions (40S, monosomes, and polysomes) in the case of

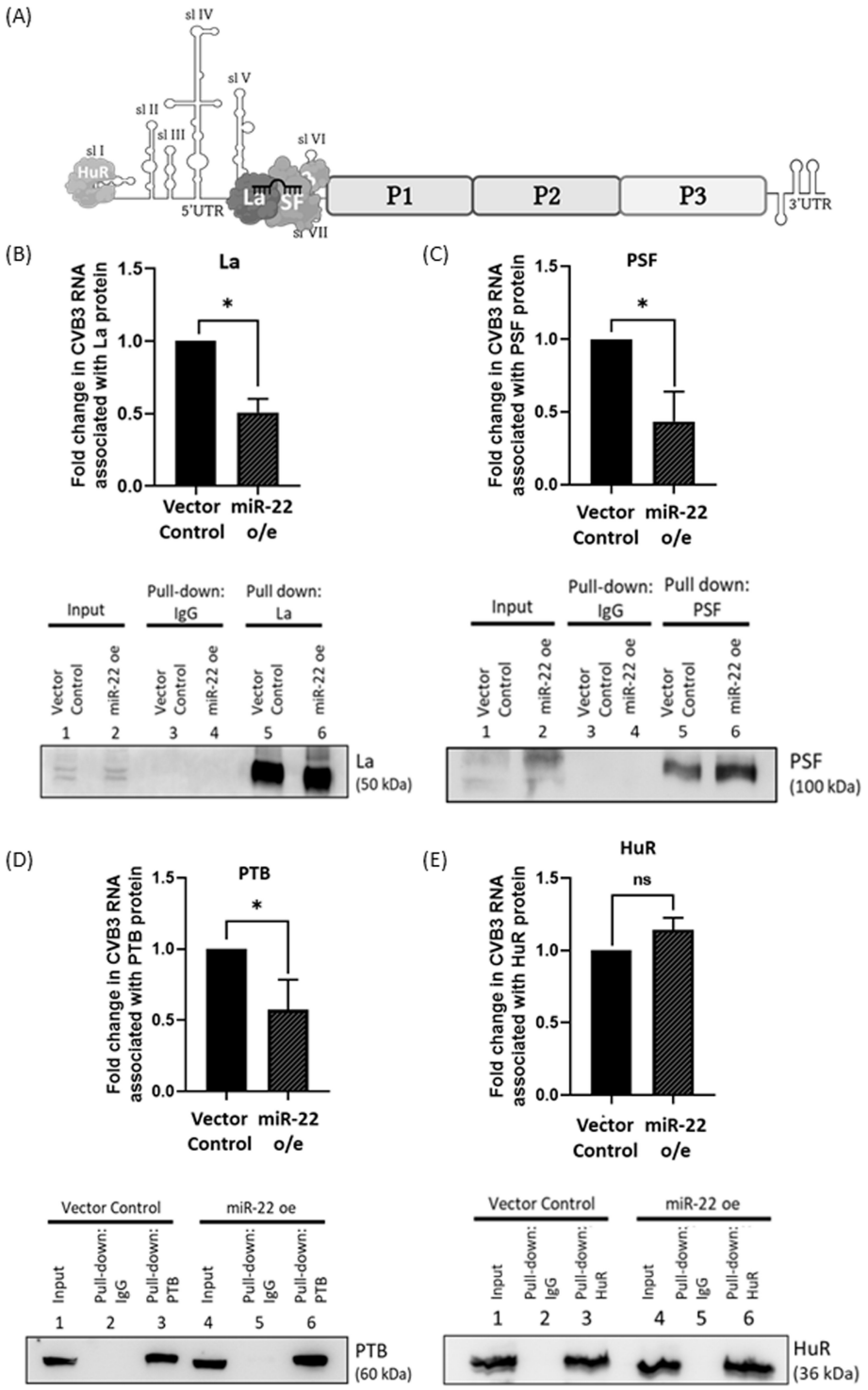

FIG 4 miR-22-3p binding to CVB3 5′ UTR displaces the ITAFs. (A) A pictorial representation of the binding site of miR-22-3p (black), La, PSF, PTB, and HuR in the CVB3 5′ UTR. (B–E) HeLa cells overexpressing miR-22-3p were infected with CVB3 (MOI 10). Cells were harvested after 8 h.p.i., and the lysate was used for immunoprecipitation using antibodies against La, PSF, PTB, and HuR. Total RNA was isolated from the total lysate, and the pull-down fractions and CVB3 RNA were quantified by qPCR. The bar graphs represent the CVB3 RNA associated with each of the proteins, normalized to the CVB3 RNA present in the total cell lysate. Western blots confirm immunoprecipitation of the respective protein. Error bars represent standard deviations in three independent experiments. *$P < 0.05$.

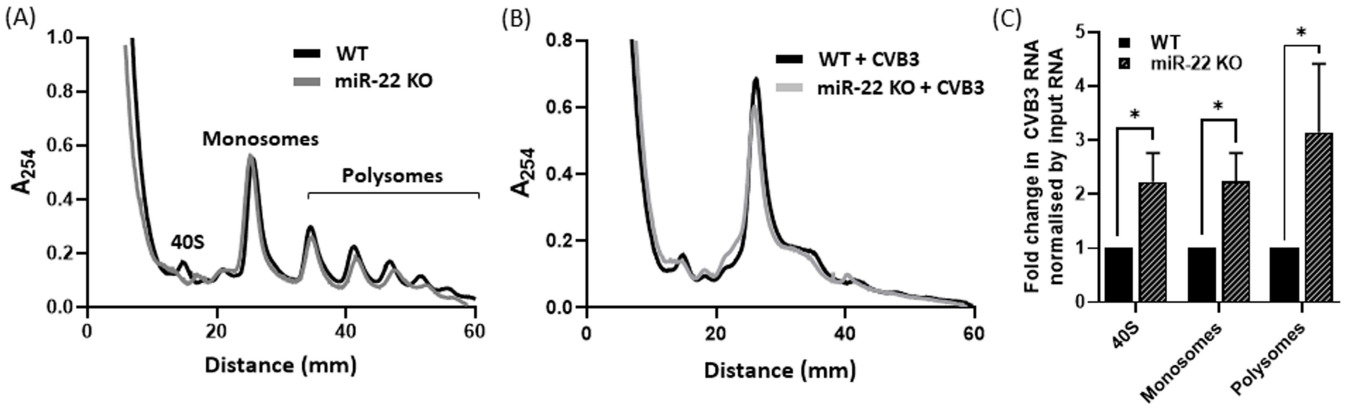

FIG 5 miR-22-3p binding to CVB3 5′ UTR inhibits ribosome recruitment. (A) Uninfected WT and miR-22-3p KO HeLa cells were used for polysome profile analysis to check the global translation profile. The profiles for WT HeLa (black) and miR-22-3p KO cells (gray) are shown. The 40S, monosome, and polysome peaks are indicated. (B) CVB3-infected WT and miR-22-3p KO HeLa cells were used for polysome profile analysis to check the global translation profile during infection. The profiles for CVB3-infected WT HeLa (black) and miR-22-3p KO cells (gray) are shown. (C) Total RNA was isolated from the 40S, monosome, and polysome fractions of the CVB3-infected WT and miR-22-3p KO cells and CVB3 RNA was quantified by qPCR. The bar graph represents the fold change in CVB3 positive strand present in the individual fractions in miR-22-3p KO cells with respect to WT HeLa cells. Error bars represent standard deviations in three independent experiments. *$P < 0.05$.

CVB3-infected miR-22-3p KO cells (Fig. 5C). These results strongly suggest that miR-22-3p hinders CVB3 RNA translation by disrupting ribosome recruitment to the internal ribosome entry site (IRES) region.

MicroRNA-22 levels increase 4 hours post-infection triggered by 2a protease

The translation of the genomic RNA strand stands out as one of the most pivotal steps in the CVB3 life cycle. Due to the absence of any viral proteins packaged within the CVB3 virion particle, the genome promptly undergoes translation upon entering the host cell's cytoplasm, enabling the synthesis of viral proteins. Notably, in HeLa cells, the initial 2 hours following CVB3 infection primarily involve CVB3 RNA translation within the cells, with robust RNA replication initiating only after 4 hours (Fig. 6A). The viral proteins play a critical role in facilitating the virus's genome replication. However, if miR-22-3p levels increase and impede CVB3 RNA translation, it could disrupt the successful progression of the infection cycle. To address this hypothesis, we examined the level of miR-22-3p at various time points post-CVB3 infection in HeLa cells. Specifically, we infected HeLa cells with CVB3 (MOI 10) and harvested the cells at 2, 4, 6, and 8 h.p.i. We confirmed CVB3 infection by quantifying CVB3 genomic RNA at different time points (Fig. 6B). Interestingly, we observed that miR-22-3p levels increased only 4 h.p.i., allowing sufficient time for viral protein synthesis to occur (Fig. 6C).

Around 4 h.p.i., the accumulation of viral proteins becomes noticeable in the cell cytoplasm (41–43) (Fig. 6D). One of these proteins is CVB3 2A protease, recognized for its involvement in the regulation of numerous host proteins, achieved through cleavage or modulation of their levels. In a recent study, we demonstrated that 2A protease, during CVB3 infection, downregulates the level of a specific miRNA, miR-125b-5p (40). This observation led us to investigate whether the increased level of miR-22-3p during CVB3 infection could be attributed to the accumulation of 2A protease. To explore this possibility, we expressed 2A protease in HeLa cells and monitored the level of miR-22-3p. In parallel, we utilized the NS3 protease from HCV as a control. The results revealed that the expression of 2A protease in HeLa cells led to an elevation in miR-22-3p levels (Fig. 6E and F). These findings strongly suggest that the levels of miR-22-3p during CVB3 infection are influenced by the presence of 2A protease.

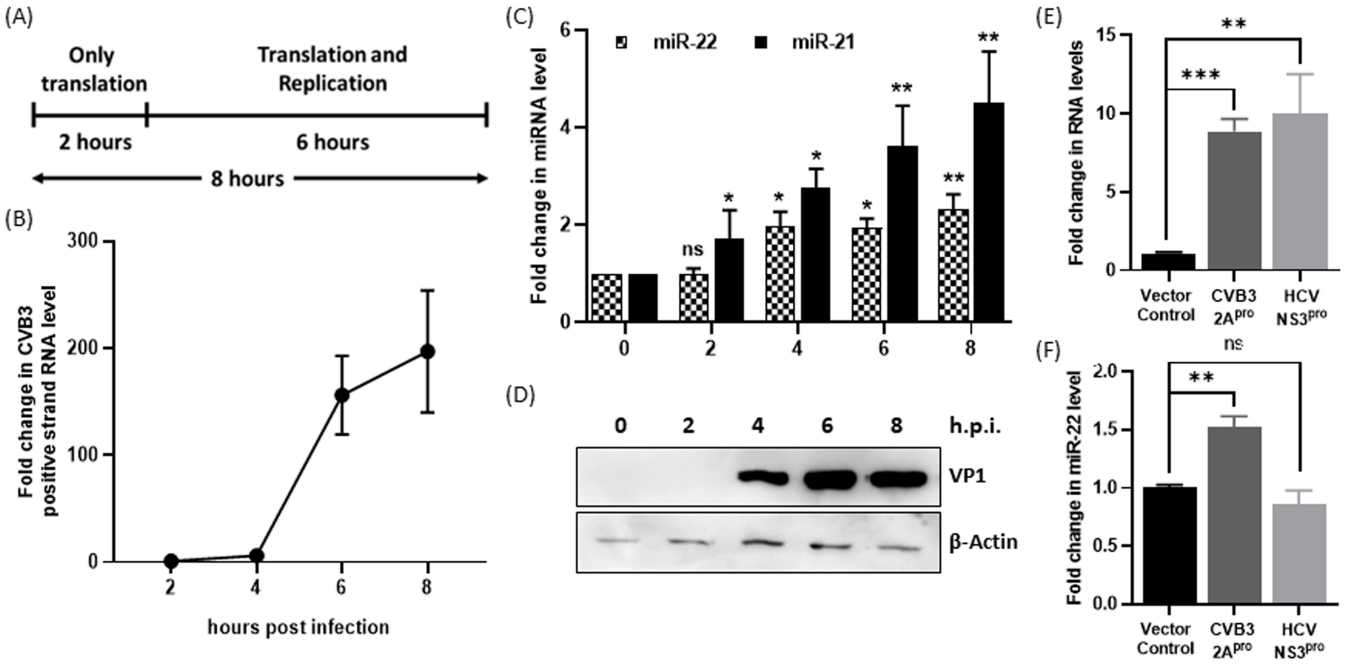

FIG 6 miR-22-3p levels increase after 4 hours of CVB3 infection as a result of $2A^{pro}$ accumulation. (A) Schematic representation of the time course of CVB3 infection in HeLa cells. For the first two hours, there is majorly CVB3 RNA translation and after that replication and translation both pickup robust speed. (B) HeLa cells seeded at a confluency of 90% were infected with CVB3 (MOI 10), and the cells were harvested 2, 4, 6, and 8 h.p.i. Total RNA was isolated and CVB3 positive-strand RNA was quantified using qPCR. (C) The levels of miR-22-3p and miR-21-5p (positive control) were detected at the different time points post-CVB3 infection. (D) Western blot represents the CVB3 VP1 protein at 2, 4, 6, and 8 h.p.i. in HeLa cells. (E) HeLa cells seeded at a confluency of 60%–70% were transfected with either pcDNA3 (vector control), CVB3 $2A^{pro}$, or HCV $NS3^{pro}$ expression plasmids, and 24 hours post-transfection, cells were harvested and total RNA was isolated. The RNA levels of CVB3 $2A^{pro}$ or HCV $NS3^{pro}$ were quantified using qPCR. (F) The bar graph represents the RNA level of miR-22-3p quantified using qPCR. Error bars represent standard deviations in three independent experiments. $*P < 0.05$, $**P < 0.01$, $***P < 0.001$.

Protocadherin-1 is regulated by miR-22-3p during CVB3 infection

Given that the increased levels of miR-22-3p during CVB3 infection are likely to impact host mRNAs targeted by miR-22-3p, we embarked on investigating its possible indirect effect on CVB3 infection. We initiated this analysis by obtaining a comprehensive list of 825 miR-22-3p targets from the miRBase database (mirbase.org). To gain insights into the functional impact of these miR-22-3p targets, we opted for pathway analysis using the Panther software (44). From the results of this pathway analysis, we identified the top three pathways and focused on the 12 genes that were shared among these pathways.

Our initial focus was on assessing the mRNA levels of the shortlisted miR-22-3p targets in response to CVB3 infection (Fig. 7A). Given that miR-22-3p is upregulated during CVB3 infection, we concentrated on the genes among the 12 targets that displayed a downregulation in response to infection for further investigation. Among these targets, we identified four genes that exhibited an inverse correlation, namely, protocadherin-1 (PCDH1), guanine nucleotide-binding protein subunit beta-4 (GNB4), TGF-beta receptor type-1, and protein Wnt-5a. The levels of these genes were checked in miR-22-3p KO cell line, for reciprocal correlation (if any). We observed that the levels of PCDH1 and GNB4 were indeed upregulated in the miR-22-3p KO cell line. Furthermore, when we subjected miR-22-3p KO cells to CVB3 infection, we found that GNB4 displayed a similar trend during infection in both the WT and miR-22-3p KO cells. However, PCDH1 exhibited an opposite trend (Fig. 7B). To gain further insights, we also assessed the level of PCDH1 in the hearts of CVB3-infected mice and found that, akin to our observations in HeLa cells, PCDH1 levels were downregulated (Fig. 7C). Collectively, these results suggest that PCDH1 might be under the regulation of miR-22-3p during CVB3 infection.

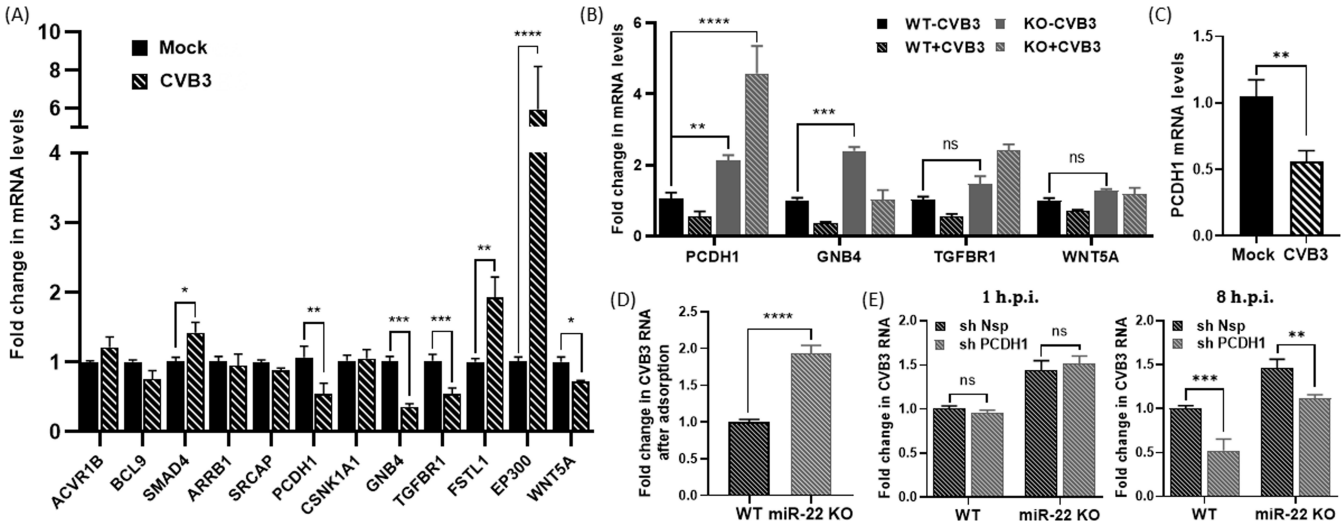

FIG 7 Protocadherin-1 is regulated by miR-22-3p during CVB3 infection and acts as a proviral factor. (A) HeLa cells seeded at a confluency of 90% were infected with CVB3 (MOI 10), and the cells were harvested at 8 h.p.i. Total RNA was isolated, and the mRNA levels of different miR-22-3p target genes were quantified by qPCR. The bar graph represents the level of mRNA targets in CVB3-infected cells versus uninfected cells. (B) WT and miR-22-3p KO HeLa cells were seeded at a confluency of 90% and were either mock-infected or CVB3-infected (MOI 10). Cells were harvested after 8 h.p.i. and total RNA was isolated. The bar graph represents the mRNA levels of PCDH1, GNB4, TGF-beta receptor type-1 (TGFBR1), and WNT5 quantified by qPCR. (C) PCDH1 mRNA levels were quantified in CVB3-infected mice heart with respect to mock-infected mice heart after 7 days of infection. (D) WT and miR-22-3p KO cells seeded at 90% confluency were infected with CVB3 (MOI 10) and harvested after 1 hour of adsorption. Total RNA was isolated, and CVB3 positive-strand RNA levels were quantified by qPCR. The bar graph represents the fold change in CVB3 that entered in miR-22-3p KO cells with respect to WT cells. (E) WT and miR-22-3p KO cells seeded at 50% confluency were transfected by either sh Nsp or sh PCDH1 plasmids and, after 24 hours, infected with CVB3 (MOI 10). Cells were harvested at 1 and 8 h.p.i., and total RNA was isolated. CVB3 RNA was quantified in the cells by qPCR. Error bars represent standard deviations in three independent experiments. *$P < 0.05$, **$P < 0.01$, ***$P < 0.001$, ****$P < 0.0001$.

Protocadherin-1 promotes CVB3 infection

The function of PCDH1 protein is reasonably underexplored. It is a single-pass transmembrane protein present in cell-cell junctions. Notably, there are two reports on PCDH1 function. The first report unveils its ability to activate nuclear factor kappa B (NF-κB) signaling in the context of pancreatic cancer (45). The second report highlights its significance in facilitating the entry of New World hantaviruses into host cells (46). Building on this background information, we formulated a hypothesis that during CVB3 infection, PCDH1 present in the vicinity of the receptors might be activated, subsequently triggering certain signaling events. Alternatively, it could serve as a co-receptor, assisting CVB3 in its entry into the host cell.

To our surprise, our investigations revealed that CVB3 entry was more efficient in miR-22-3p KO cells as compared to WT HeLa cells (Fig. 7D). Motivated by this observation, we opted to partially silence PCDH1 in miR-22-3p KO cells to evaluate its impact on CVB3 infection. PCDH1 mRNA levels were checked to confirm partial silencing (data not shown). Interestingly, we found that while PCDH1 knockdown did not manifest an effect on CVB3 infection during the early stages of infection, it significantly downregulated CVB3 infection during the later phases of infection (see Fig. 7E). These results provide compelling evidence indicating that PCDH1 indeed plays a role in promoting CVB3 infection.

MicroRNA-22 levels post-infection determine the virus replication in various organs

Having established the direct and indirect roles of miR-22-3p in CVB3 infection, we were keen to explore whether this microRNA played a part in determining tissue or organ tropism during CVB3 infection. miR-22-3p exhibits differential expression across various

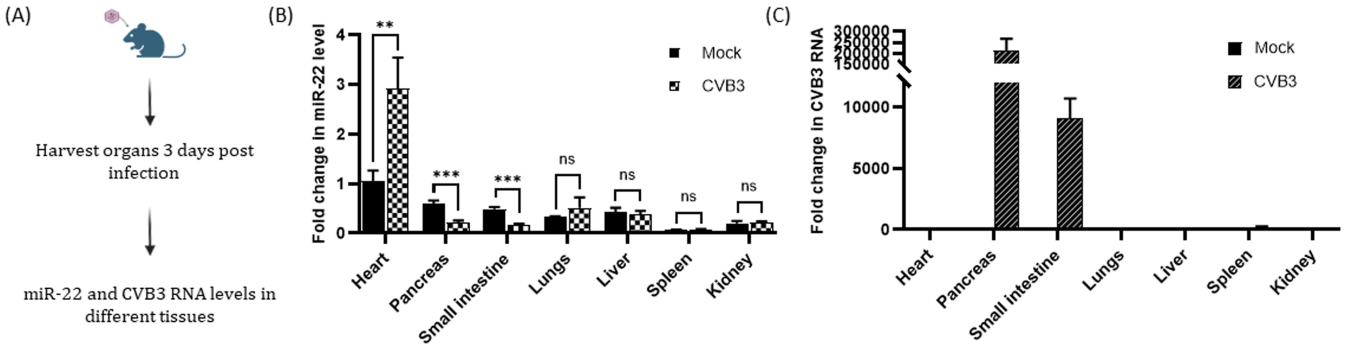

FIG 8 miR-22-3p levels determine the level of CVB3 infection in different organs. (A) A schematic representation of the workflow for the consecutive experiment. Three- to four-week-old male BALB/c were either mock-infected or CVB3-infected (10^5 PFU). The animals were sacrificed at 3 d.p.i. and different organs were harvested. Total RNA was isolated from the different tissues and miR-22-3p, and CVB3 RNA levels were quantified using qPCR. (B) The bar graph represents the level of miR-22-3p in different organs of mock and CVB3-infected mice with respect to mock-infected mice heart. (C) The bar graph represents the level of CVB3 positive-strand RNA detected in different organs 3 d.p.i. Error bars represent standard deviations in five biological replicates. $^{**}P < 0.01$, $^{***}P < 0.001$.

organs in the body, with particularly high expression levels in the heart. Additionally, different cell types possess distinct cellular environments, which contribute to their unique responses to viral infections. Hence, it is conceivable that upon infection, different organs may exhibit varied regulations of miR-22-3p, ultimately influencing the proliferation of CVB3 in these organs.

To delve into this question, we conducted an experiment involving 3- to 4-week old male BALB/c mice. We infected them with 10^5 PFU of CVB3 or subjected them to a mock treatment with phosphate-buffered saline (PBS), serving as a control. After 3 d.p.i., we sacrificed the mice and harvested various organs (Fig. 8A). We assessed the levels of miR-22-3p and CVB3 RNA in different organs. As anticipated, we observed elevated levels of miR-22-3p in the heart tissue of CVB3-infected mice. Intriguingly, we found that miR-22-3p was downregulated in the small intestine and pancreas post-infection, coinciding with high levels of CVB3 RNA. In contrast, miR-22-3p levels remained unchanged in the remaining organs (Fig. 8B and C).

DISCUSSION

The infection caused by CVB3 presents a paradigm where miRNAs play pivotal roles in distinct phases. miRNAs can directly target viral mRNA or host genes, thereby impacting the course of infection. While considerable evidence underscores the indirect contribution of miRNAs to CVB3 infection, limited information is available on the host miRNAs that bind directly to CVB3 RNA. In this study, we elucidated the involvement of miR-22-3p in the intricate network governing CVB3 infection, adding a novel facet to the regulatory landscape.

miR-22-3p expression undergoes modulation in response to various viral infections, including hepatitis B virus (HBV), HIV, HCV, influenza A virus, porcine reproductive and respiratory syndrome virus (PRRSV), H1N1, Japanese encephalitis virus (JEV), and transmissible gastroenteritis coronavirus (47–54). Across multiple viral infections, miR-22-3p exhibits a proviral role. For instance, in PRRSV infection, miR-22-3p promotes viral replication by targeting heme oxygenase-1, an anti-viral factor (50). In the case of JEV infection, miR-22-3p targets MAVS, resulting in diminished interferon (IFN)1 production and facilitating viral replication (52). During lymphocytic choriomeningitis virus (LCMV) infection, miR-22-3p enhances the IFN response, thereby contributing to enhanced disease severity. Interestingly, KO mice lacking miR-22-3p survived a lethal viral dose due to reduced IFN-alpha production (55). Reports also suggest a potential association between miR-22-3p and HBV-related hepatocellular carcinoma, regarding its impact on HepB e antigen and hepatitis B surface antigen (47). However, none of the reports proposed a direct interaction between miR-22-3p and viral RNA.

Our investigation primarily focuses on the role of miR-22-3p during CVB3 infection, where it binds to the CVB3 5′ UTR and substantively influences both CVB3 RNA translation and host mRNA, specifically PCDH1. The process of miR-22-3p binding to the CVB3 5′ UTR entails inhibiting CVB3 infection. Along with miR-22-3p, we used miR-21-5p overexpression and knockdown as a control. miR-21-5p is known to have no impact on CVB3 RNA translation and replication. However, it shows significant negative regulation of CVB3 virus particle release (13). Unlike miR-21-5p, miR-22-3p showed a deleterious effect on all virus processes. The binding of miR-22-3p to CVB3 5′ UTR spatially hampers the binding of critical ITAFs, namely, PSF, PTB, and La protein, which share binding motifs within the CVB3 RNA 5′ UTR with miR-22-3p. These proteins are acknowledged for promoting CVB3 RNA translation, including ribosomal recruitment to the IRES. The coordinated binding of these proteins contributes to efficient viral protein synthesis. After analyzing the results, we concluded that the effect of miR-22-3p was majorly on CVB3 RNA translation, and the effect observed on other processes such as replication and virus production is an indirect consequence. It is noteworthy that the sequence from stem loops V to VI demonstrates a high degree of conservation across all Coxsackievirus B serotypes and not just CVB3 strains. Furthermore, the binding site of miR-22-3p in the UTR lacks overlap with any other microRNA, underscoring the specificity of this interaction. Importantly, around 4 hours post-infection, miR-22-3p expression increases, coinciding with the accumulation of viral proteins, 2A protease being one of them. While the exact mechanism by which 2A protease enhances miR-22-3p levels is unknown, it can be speculated that it might directly or indirectly increase the promoter activity. A detailed investigation is required to decipher this mechanism. This temporal increase in miR-22-3p potentially enhances its prospect for binding to CVB3 RNA. The ensuing miR-22-3p binding to the 5′ UTR causes displacement of ITAFs, effectively attenuating the translational process (Fig. 9). Since the binding of miR-22-3p seed sequence and CVB3 RNA is not completely complementary, we do not suspect that miR-22-3p is also involved with degrading CVB3 RNA.

Moreover, the increased miR-22-3p level subsequently impacts host target genes, exemplified by the reduced expression of PCDH1. PCDH1 in an underexplored protein. It is a transmembrane protein, which is majorly located in cell-cell junctions. A report suggests the involvement of PCDH1 in activating NF-κB signaling in pancreatic ductal adenocarcinoma (45). During CVB3 infection, NF-κB signaling is known to be activated in HeLa cells (56). However, in contrast, a recent study in peritoneal macrophages shows that NF-κB signaling is suppressed upon CVB3 infection (57). Another study showed that PCDH1 is involved in New World hantaviruses' entry into host cells (46). CVB3 utilizes decay accelerating factor (DAF) or CD55 as an attachment receptor and Coxsackievirus and adenovirus receptor (CAR) as an uncoating receptor. However, CVB3 has been known to modulate the receptor requirements based on availability. Moreover, while the use of DAF and CAR in CVB3 entry has been characterized, the possible involvement of other proteins as co-receptors cannot be ruled out (58). Our results suggested a proviral role of PCDH1 during CVB3 infection. A detailed study on PCDH1 during CVB3 infection will enlighten on how it helps the virus during infection: by regulating cellular signaling or acting as a co-receptor for viral entry (Fig. 9).

This phenomenon invites inquiry into the rationale behind suicidal induction of an anti-viral miRNA by the virus. Two plausible hypotheses may elucidate this phenomenon. Firstly, it is speculated that the CVB3 2A protease does not directly cause the increase in miR-22-3p levels. Instead, this protease is recognized by another protein as a potential threat to the host, thereby initiating a cascade of events culminating in the induction of miR-22-3p. Subsequently, miR-22-3p assumes the role of an anti-viral molecule by inhibiting viral translation and facilitating the degradation of the proviral host factor, PCDH1. However, a comprehensive investigation is required to ascertain the existence, if any, of intermediate proteins involved in this process. Alternatively, CVB3 augments miR-22-3p levels for its strategic benefit. The RNA strand utilized for translation is concurrently utilized for replication. The continuous occupation of CVB3 RNA by

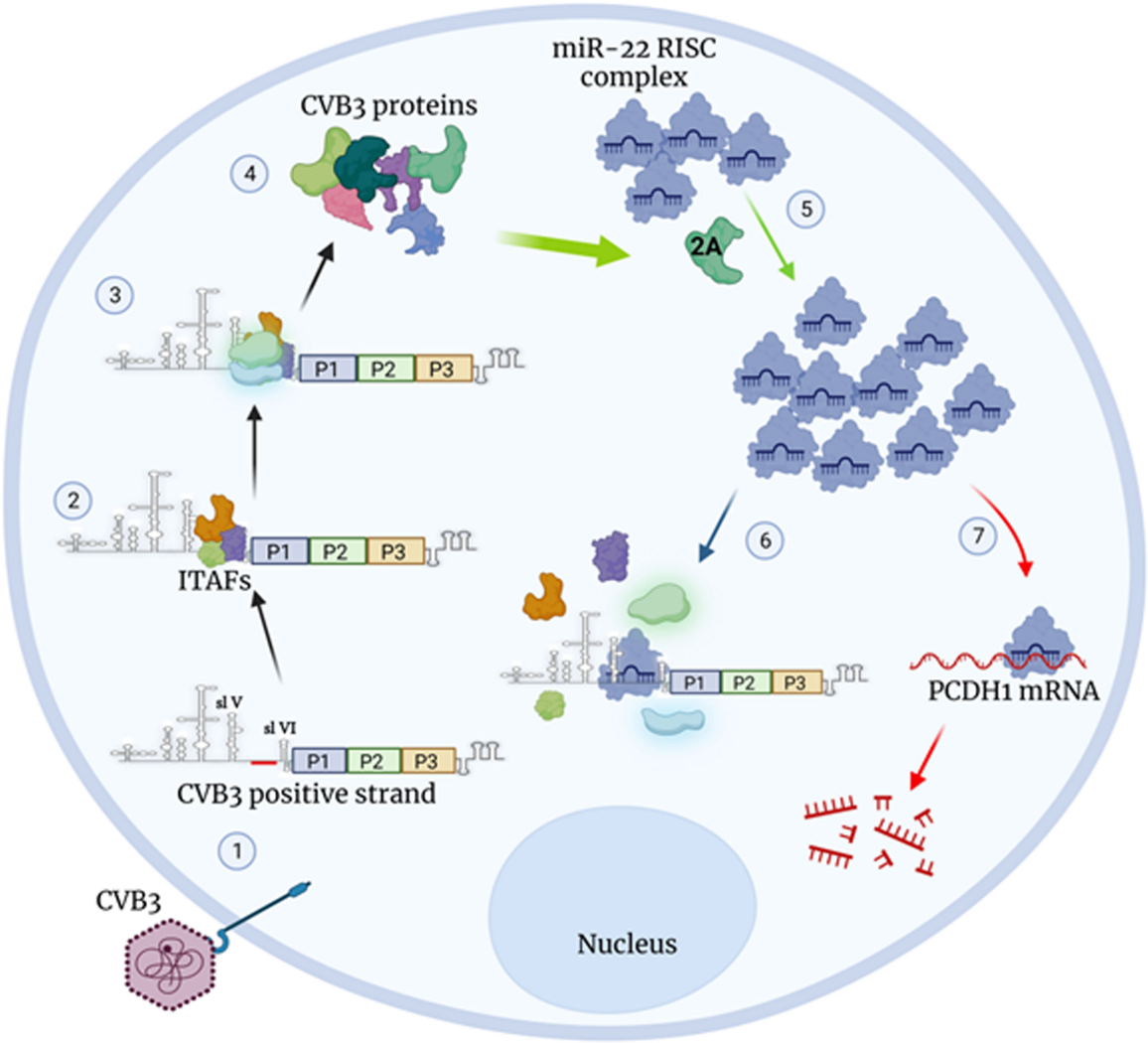

FIG 9 Model. Dual role of miR-22-3p during CVB3 infection. (1) Upon CVB3 infection, the genomic RNA is released into the host cell cytoplasm, (2) which is then bound by different ITAFs such as La, PSF, and PTB. (3) This leads to ribosome recruitment and viral RNA translation (4) to synthesize CVB3 proteins. (5) The accumulation of viral 2A protease in the cytoplasm acts as a trigger for enhancing the levels of miR-22-3p. The exact mechanism by which $2A^{pro}$ induces miR-22-3p levels is unclear. (6) miR-22-3p now displaces the ITAFs bound to the CVB3 5′ UTR, inhibiting its translation. (7) The indirect effect of miR-22-3p during CVB3 infection is by targeting PCDH1. During CVB3 infection, PCDH1 acts as a proviral host factor. However, the increased level of miR-22-3p upon CVB3 infection downregulates PCDH1 and inhibits its function (created with BioRender.com).

translation-promoting factors hampers the seamless transition from translation to replication. Elevating miR-22-3p levels potentially facilitates this transition, promoting replication. However, miR-22-3p subtly exploits this scenario to wield an anti-viral effect by repressing proviral PCDH1. This dual nature of miR-22-3p's function intricately weaves into CVB3's regulatory strategy, representing a dichotomous relationship where the virus benefits from miR-22-3p elevation for replication while simultaneously grappling with its anti-viral repercussions.

An additional layer of complexity emerges through the tissue-specific expression patterns of miR-22-3p, provoking in-depth investigation into its potential role in determining CVB3's tissue/organ tropism. The levels of miR-22-3p in small intestine and pancreas are moderate. However, to our surprise, upon CVB3 infection in mice, miR-22-3p levels were downregulated in both small intestine and pancreas. The small intestine is the primary target organ of CVB3 (59). Apart from miR-22-3p, the level of PCDH1 protein is also highest in the different organs of the gastrointestinal tract (Human Protein Atlas, proteinatlas.org) (60). Pancreas, a secondary target organ of CVB3, harbors

high La protein, which helps in viral RNA translation, hence aiding in viral proliferation (28). The combined effect of low level of anti-viral molecule and high level of proviral molecule makes the small intestine and pancreas appropriate organs to be targeted. This intriguing observation indicates miR-22-3p's and its target's potential influence in the virus's selection of the small intestine as a preferred site for primary infection. Furthermore, CVB3 attacks pancreas next, which provides another favorable environment for it to replicate robustly. This hypothesis gains additional support from the observation that the site to which miR-22-3p binds exhibits a high degree of conservation among Coxsackieviruses. Conversely, the host responds to viral attack by signaling the heart, another secondary target organ, to increase the levels of anti-viral molecules, such as miR-22-3p, as a protective measure against severe viral infection. Since cardiomyocytes are terminally differentiated, it is essential to protect them from any possible cell death, which in this case, might be the viral infection. This underscores the ongoing evolutionary arms race between the host and the virus, illustrating their adaptive strategies to overcome challenges and maintain relevance.

Overall, this investigation has unraveled the multifaceted role of miR-22-3p in regulating CVB3 infection, which can be harnessed for designing miRNA-based therapies. miR-22-3p-based therapy would offer a multidimensional therapeutic approach through direct binding to the CVB3 5′ UTR, culminating in the inhibition of viral RNA translation, while its capacity to suppress proviral PCDH1 attests to its anti-viral potency. miR-22-3p mimics (pre-miRNAs) can be supplemented into the host using nucleic acid delivery systems, thereby increasing miRNA load attenuating CVB3 infection and its related diseases.

The dynamic regulation of miR-22-3p during infection underscores its intricate involvement in CVB3 pathogenesis. One pivotal aspect of our research is the delineation of time-dependent regulation of various host factors contributing to CVB3's establishment of a successful infection cycle. In this intricate puzzle, miR-22-3p plays a modest yet essential part.

MATERIALS AND METHODS

Cell lines and transfections

HeLa cells were maintained in DMEM (Sigma) supplemented with 10% fetal bovine serum (FBS) (GIBCO, Invitrogen) and antibiotics. For transfection, 50% or 90% confluent monolayer of cells (depending on the experiment) was transfected with various plasmid constructs or RNAs using Lipofectamine 2000 (Invitrogen) or turbofectamine in Opti-MEM (Invitrogen). Following a 5-hour incubation period, the culture medium was replaced with DMEM containing antibiotics and 10% FBS. Subsequently, at the designated time points, the cells were harvested and processed according to the specific requirements of the experiments.

Plasmids and RNAs

pRib-CB3/T7-LUC construct was used for the preparation of CVB3 subgenomic replicon RNA. The construct linearized with SalI enzyme was used for *in vitro* transcription reactions using T7 polymerase as per manufacturer's protocol.

pRib-CB3/T7 construct was used for the preparation of CVB3 infectious virus (Nancy strain). The construct linearized with MluI enzyme was used for *in vitro* transcription reactions using T7 polymerase as per manufacturer's protocol.

pSUPER-miR-22-3p and pSUPER-miR-21-5p constructs were used to overexpress miR-22-3p and miR-21-5p, where the miRNA sequence was cloned between BglII and XhoI sites in pSUPER vector.

AntimiR-22-3p (mirVana miRNA inhibitor for hsa-miR-22-3p, assay ID MH10203) or anti-miR-21-5p (mirVana miRNA inhibitor for hsa-miR-21-5p, assay ID MH10206) RNAs were used for partial silencing of miR-22-3p and miR-21-5p, respectively.

CVB3 2A protease and HCV NS3 protease overexpression constructs were cloned in pcDNA3.1 vector.

For preparation of CVB3 5′ UTR-FLuc, CVB3 5′ UTR-FLuc-3′ UTR, and FLuc-CVB3 3′ UTR RNA, respective sites were cloned in pcDNA3.1 vector. The clones were already available in the laboratory.

Preparation of CVB3 infectious virus

The pRiB-T7-CB3 plasmid (a generous gift from Prof. Nora Chapman) containing CVB3 cDNA was used for infectious viral RNA preparation. This RNA was transfected into HeLa cells for CVB3 virus production. After 2–3 days of incubation, cells were lysed by three cycles of freeze-thawing, and the cell suspension was collected in a 15-mL tube. Dead cells and cellular debris were removed by centrifugation at 5,000 rpm for 10 minutes at 4°C. The supernatant containing the CVB3 virus was collected and aliquoted before being stored at −80°C to maintain its infectivity. Freshly prepared virus was used to estimate plaque-forming units per milliliter using plaque assay in Vero cells.

Site-directed mutagenesis

CVB3 5′ UTR primers (Table 1) were designed incorporating mutations at the nucleotide position 587 (G–C) and 588 (C–G), followed by PCR amplification using the WT CVB3 5′ UTR as template. The PCR product was then treated with Dpn1 to digest the methylated template DNA. Bacterial transformation using DH5α strain was done using the digested PCR product, and the resultant colonies were screened by sequencing.

Virus infection in cell line

Cells were seeded at 90% confluency and before infection, washed with DMEM media without FBS. The required amount of virus was diluted in DMEM (without serum) and added to the cells. The dish was them swirled gently at regular intervals of 10 minutes for 45 minutes to 1 hour. This is the adsorption step. Next, remaining virus is removed, and fresh growth media is added to the cells.

Virus infection in mice

Three- to four-week old male BALB/c mice were either injected with PBS for mock infection or CVB3 intraperitoneally. The mice were sacrificed 3 or 7 days post-infection, and the organs were harvested.

TRAP assay

The method is based on adding MS2 RNA hairpin loops to a target RNA of interest, followed by co-expression of the MS2-tagged RNA together with the protein MS2 (which recognizes the MS2 RNA elements) fused to an affinity tag (61). After purification of the MS2 RNP complex, the miRNAs present in the complex are identified. In this study, we have tagged the CVB3 5′ UTR (WT or mutant) with MS2 hairpins and have co-expressed it in HeLa cells along with the chimeric protein MS2-GST (glutathione S-transferase). After affinity purification using glutathione SH beads, the microRNAs present in the RNP complex were detected by qPCR.

miR-22-3p knockout cell line generation

pspCas9(BB)-2A-GFP(PX458) vector was used to clone miR-22-3p-specific gRNAs. The clones were transfected in HeLa cell lines, and 48 hours post-transfection, GFP-expressing cells were sorted in a 96-well plate by single cell sorting using fluorescence-activated cell sorting (FACS). The sorted cells were propagated and further miR-22-3p knockout clones were screened and validated by sequencing and qPCR.

TABLE 1 Primers used in the study

CVB3_UTR_460 F	GAATGCGGCTAATCCTAACTGC
CVB3_UTR_655 R	GCTCTATTAGTCACCGGATGGC
Human GAPDH F	CAGCCTCAAGATCATCAGCAAT
Human GAPDF R	GGTCATGAGTCCTTCCACGA
Mouse GAPDH F	TGCAGTGGCAAAGTGGAGATT
Mouse GAPDH R	TTGAATTTGCCGTGAGTGGA
CVB3 miR22 SDM F	TTCCTATACTGGCTCGTTATGGTGACAATTG
CVB3 miR22 SDM R	CAATTGTCACCATAACGAGCCAGTATAGGAA
miR-22 CRISPR g1 F	GAACTGTTGCCCTCTGCCCCGTTTT
miR-22 CRISPR g1 R	GGGGCAGAGGGCAACAGTTCCGGTG
miR-22 CRISPR g2 F	GAGCCGCAGTAGTTCTTCAGGTTTT
miR-22 CRISPR g2 R	CTGAAGAACTACTGCGGCTCCGGTG
PCDH1 qPCR F	TGAGGCCCAGGAGCTATTTG
PCDH1 qPCR R	TTCACCTGGATGACCGAGTG
ACVR1B qPCR F	TCTCCAAAGACAAGACGCTCC
ACVR1B qPCR R	GGATGTTTTCATGGCGCAGC
ARRB1 qPCR F	GGAAAGCGGGACTTTGTGGA
ARRB1 qPCR R	TCGCCCAGCTTCTTGATGAG
WNT5A qPCR F	TTTCTCCTTCGCCCAGGTTG
WNT5A qPCR R	GTGGTCCTGATACAAGTGGCA
EP300 qPCR F	AGGGGACATGTATGAATCTGCAA
EP300 qPCR R	GCACACTGCCACGGATCATA
TGFBR1 qPCR F	AACCGCACTGTCATTCACCA
TGFBR1 qPCR R	CAACTTCTTCTCCCCGCCA
FSTL1 qPCR F	TGGCTGGTTCTCTAAAGGCAG
FSTL1 qPCR R	GATGGGTTGAGGCACTTGAG
SRCAP qPCR F	ACAGGCGTGGTGAAGATTGT
SRCAP qPCR R	GGACTGTGGACCAGCTTGAG
CSNK1A1 qPCR F	AGCAGCGGCTCCAAGG
CSNK1A1 qPCR R	TGCTCTCGTACAGCAACTGG
GNB4 qPCR F	GGACAGGCCTCATTTTTGGC
GNB4 qPCR R	AGGCCCTTTTGCTGTTGAGA
SMAD4 qPCR F	TCCTGTGGCTTCCACAAGTC
SMAD4 qPCR R	CAGTCCAGGTGGTAGTGCTG
BCL9 qPCR F	AGTCCTGGGATCCCTCCAAA
BCL9 qPCR R	GAGCTGGCCACAGTCTTGAT

MTT assay

HeLa cells were transfected with pSUPER only, pSUPER-mir22, pSUPER-mir21 overexpression constructs or with Nsp anti-miR, anti-miR-22-3p, or anti-miR-21-5p, and MTT was added to the media 24 hours post-transfection. After 3 hours of incubation, media were removed and cells were dissolved in DMSO, followed by measurement of absorbance at 550 nm.

In vitro transcriptions

RNA synthesis was performed *in vitro* using linearized constructs containing the T7 promoter. Two plasmids, pRib-CB3/T7-LUC and pRIB-CB3/T7, were used, and they were linearized with SalI and MluI enzymes, respectively. The linearized DNA was then ethanol-precipitated and used as a template for RNA synthesis using T7 RNA polymerase (Fermentas). The transcription reactions were carried out under standard conditions (Fermentas protocol) using 1 µg of linearized template DNA at 37°C for 4 hours. After ethanol precipitation, RNAs were resuspended in nuclease-free water.

Luciferase assays

Transfected cells were harvested and lysed using 1× passive lysis buffer (Promega). Cell lysates were centrifuged at 10,000 rpm for 10 minutes at 4°C. Supernatant was collected and used for taking the luciferase reading using Dual Luciferase kit (Promega) as per manufacturer's protocol. Readings were normalized to total protein.

Western blot analysis

The protein concentration from cell lysates was quantified using the Bradford method. Equal amounts of protein were separated on 12% denaturing PAGE gels and transferred to a nitrocellulose membrane (Pall Biosciences). The analysis of these proteins was conducted using specific antibodies.

RNA isolation

Total RNA was extracted from cells at various time points using TRI Reagent (Sigma) following the standard protocol. After trypsin digestion, the cells were collected using PBS, and 250 µL of TRI reagent was added to the cell pellet for proper lysis. Subsequently, 50 µL of chloroform was introduced to the tubes containing the lysed cells in TRI reagent. After vigorous vertexing for 30 seconds, the tubes were centrifuged at 12,000 rpm for 20 minutes. The resulting supernatant was collected, and RNA precipitation was carried out by adding an equal volume of isopropanol. The RNA pellet was then washed with 70% ethanol (or 80% ethanol for miRNA quantification). Following this, DNaseI digestion was performed at 37°C for 30–45 minutes. Next, an equal volume of phenol:chloroform (1:1 ratio) was added to the solution, vortexed, and centrifuged at 10,000 rpm for 10 minutes. To the resulting supernatant, absolute ethanol (2.5 volumes), sodium acetate pH 5.2 (one-tenth of the volume), and glycogen were added, and the mixture was kept at −80°C overnight for precipitation. After the overnight precipitation, the pellet was washed with 70% ethanol (or 80% ethanol for miRNA experiments), briefly air-dried, and then resuspended in DEPC-treated water.

cDNA synthesis and qPCR

For CVB3 RNA and host mRNAs, cDNA was synthesized using Moloney Murine Leukemia Virus Reverse Transcriptase (MMLV RT) (RevertAid First Strand cDNA Synthesis Kit, Thermo Scientific), according to standard protocol. Total RNA of 600 ng was incubated with the specific reverse primer in RT buffer at 75°C for 5 minutes, followed by snap chilling on ice. Appropriate amount of RT buffer, 10-mM dNTP mix and reverse transcriptase enzyme was added to the mixture, and reverse transcription was performed at 42°C for 1 hour, followed by 75°C for 10 minutes for enzyme inactivation. This was used as a template for the quantitative PCR using specific forward and reverse primers for the respective genes.

For miRNAs, TaqMan microRNA Assay System was used for miR-22-3p (assay ID 000398) and miR-21-5p (assay ID 000397) quantification. Reverse transcription was performed using the kit reagents using 10 ng of total RNA per reaction. Reaction conditions used were 16°C for 30 minutes, 42°C for 30 minutes, and 85°C for 5 minutes. qPCR was performed in 10-µL reaction volume as per the protocol in TaqMan MicroRNA Assay Kit for 40 cycles. RNU6B (assay ID 001093) was used as an internal control.

RNA immunoprecipitation

For RNA immunoprecipitation (RNA-IP), cells were transfected with CVB3 replicon RNA and were lysed 8 hours post-transfection with buffer containing 100-mM KCl, 5-mM $MgCl_2$, 10-mM HEPES (4-(2-hydroxyethyl)-1-piperazineethanesulfonic acid) (pH 7.0), 0.5% NP-40, 1-mM DTT (dithiothreitol), and 100-U/mL RNase inhibitor. An equal amount of lysate was then incubated for 4 hours with protein G beads that had been pre-saturated with specific antibodies to form RNP complexes. Subsequently, the RNP complexes were washed thrice with the IP buffer, and the beads were resuspended in

the same buffer. A 10% aliquot of this resuspended mixture was used for the analysis of proteins through Western blotting, while the remaining portion was treated with 30 µg of proteinase K in the presence of 0.1% SDS at 50°C for 30 minutes. Following this treatment, Trizol was added to these reactions for RNA isolation. The isolated RNA was then utilized for qPCR.

Polysome profiling

The wild type or miR22 knockout HeLa cells were cultured in 100-mm dishes and infected with CVB3 virus. After 8 hours of incubation, the cells were treated with cycloheximide (100 µg/mL) for 10 minutes at 37°C. Following this, the cells were washed with ice-cold PBS containing cycloheximide and then with hypotonic buffer [5-mM Tris-HCl (pH 7.5), 1.5-mM KCl, 5-mM $MgCl_2$, and 100-µg/mL cycloheximide]. The cells were then scraped in ice-cold lysis buffer [5-mM Tris-HCl (pH 7.5), 1.5-mM KCl, 5-mM $MgCl_2$, 100-µg/mL cycloheximide, 1-mM DTT, 200-U/mL RNasin, 200-µg/mL tRNA, 0.5% Triton X-100, 0.5% sodium deoxycholate, and 1× protease inhibitor cocktail] and kept on ice for 15 minutes. After 15 minutes, the lysate's KCl concentration was adjusted to a final concentration of 150 mM. The cell lysate was then centrifuged at 3,000 × *g* for 8 minutes at 4°C, and the resulting supernatant was collected and either processed immediately or flash frozen and stored at −80°C for later use. Subsequently, 1.0–1.5 µg of total protein was loaded onto a 10%–50% sucrose gradient and centrifuged at 36,000 rpm for 2 hours at 4°C using an SW41 rotor (Beckman). Polysome profiles were visualized, and the fractions were collected using a polysome profiler (BioComp). Individual fractions were then used for RNA isolation and qPCR.

Statistical analysis

All the experiments are performed in three independent biological replicates. Statistical significance was determined using two-tailed Student's *t*-test.

ACKNOWLEDGMENTS

We thank Frank van Kuppeveld and Nora Chapman for various constructs; the Centre for Infectious Disease Research, Indian Institute of Science (IISc), for allowing the use of the biosafety level 3 facility; and the Biological Science Department, IISc, for the use of the FACS facility. We also thank Dr. Deepak Saini, Department of Molecular Reproduction, Development and Genetics, IISc, for providing the HeLa cell line; Dr. Umesh Varshney, Department of Microbiology and Cell Biology, for allowing the usage of laboratory facilities for polysome analysis.

P.R., B.G., and S.D.: conception and design of studies, analysis, and interpretation; P.R. and S.D.: article writing; P.R., B.G., S.V., S.B., R.S., M.V., and A.P.: performing the experiments.

P.R., S.V., and A.P. are supported by the Ministry of Human Resource Development. S.B. and M.V. are funded by the Department of Biotechnology (DBT), India. Funding was provided by a D.S. Kothari fellowship from University Grants Commission, Government of India, to B.G. Financial help from DBT-IISc Partnership Program is also acknowledged. S.D. acknowledges the JC Bose fellowship from Department of Science and Technology, Government of India. The work was also supported by a research grant from Department of Biotechnology, Government of India.

AUTHOR AFFILIATIONS

[1]Department of Microbiology and Cell Biology, Indian Institute of Science, Bangalore, India
[2]Molecular Biophysics Unit, Indian Institute of Science, Bangalore, India
[3]National Institute of Biomedical Genomics, Kalyani, India

AUTHOR ORCIDs

Priya Rani http://orcid.org/0009-0000-9457-5638
Saumitra Das http://orcid.org/0000-0002-0640-3586

FUNDING

Funder	Grant(s)	Author(s)
Ministry of Education, India (MoE)		Priya Rani V Sabarishree Apala Pal
University Grants Commission (UGC)		Biju George
Department of Biotechnology, Ministry of Science and Technology, India (DBT)		Somarghya Biswas V Madhurya
DST | Science and Engineering Research Board (SERB)		Saumitra Das
Department of Biotechnology, Ministry of Science and Technology, India (DBT)		Saumitra Das

AUTHOR CONTRIBUTIONS

Priya Rani, Conceptualization, Data curation, Formal analysis, Investigation, Methodology, Project administration, Validation, Writing – original draft | Biju George, Conceptualization, Data curation, Methodology, Writing – review and editing | Sabarishree V, Data curation | Somarghya Biswas, Data curation | Madhurya V, Data curation | Raju S. Rajmani, Data curation | Saumitra Das, Conceptualization, Funding acquisition, Methodology, Project administration, Resources, Supervision, Writing – review and editing.

DATA AVAILABILITY

Data available within the article.

ETHICS APPROVAL

The mice study was approved by the Institutional Animal Ethics Committee [Central Animal Facility (CAF)/Ethics/720/2019]. Mice were obtained from CAF, Indian Institute of Science. The experiment was carried out according to the Committee for the Purpose of Control and Supervision of Experiments on Animals and ARRIVE guidelines in the Virus BSL-3 Laboratory at the Centre for Infectious Disease Research, Indian Institute of Science, Bangalore, India.

REFERENCES

1. Harris KG, Coyne CB. 2014. Death waits for no man--does it wait for a virus? How enteroviruses induce and control cell death. Cytokine Growth Factor Rev 25:587–596. https://doi.org/10.1016/j.cytogfr.2014.08.002
2. Garmaroudi FS, Marchant D, Hendry R, Luo H, Yang D, Ye X, Shi J, McManus BM. 2015. Coxsackievirus B3 replication and pathogenesis. Future Microbiol 10:629–653. https://doi.org/10.2217/fmb.15.5
3. Alirezaei M, Flynn CT, Wood MR, Whitton JL. 2012. Pancreatic acinar cell-specific autophagy disruption reduces Coxsackievirus replication and pathogenesis *in vivo*. Cell Host & Microbe 11:298–305. https://doi.org/10.1016/j.chom.2012.01.014
4. Fairweather D, Stafford KA, Sung YK. 2012. Update on Coxsackievirus B3 myocarditis. Curr Opin Rheumatol 24:401–407. https://doi.org/10.1097/BOR.0b013e328353372d
5. Zhang C, Xiong Y, Zeng L, Peng Z, Liu Z, Zhan H, Yang Z. 2020. The role of non-coding RNAs in viral myocarditis. Front Cell Infect Microbiol 10:312. https://doi.org/10.3389/fcimb.2020.00312
6. Hemida MG, Ye X, Zhang HM, Hanson PJ, Liu Z, McManus BM, Yang D. 2013. MicroRNA-203 enhances Coxsackievirus B3 replication through targeting zinc finger protein-148. Cell Mol Life Sci 70:277–291. https://doi.org/10.1007/s00018-012-1104-4
7. Germano JF, Sawaged S, Saadaeijahromi H, Andres AM, Feuer R, Gottlieb RA, Sin J. 2019. Coxsackievirus B infection induces the extracellular release of miR-590-5p, a proviral microRNA. Virology 529:169–176. https://doi.org/10.1016/j.virol.2019.01.025
8. Ye X, Hemida MG, Qiu Y, Hanson PJ, Zhang HM, Yang D. 2013. MiR-126 promotes Coxsackievirus replication by mediating cross-talk of ERK1/2 and Wnt/β-catenin signal pathways. Cell Mol Life Sci 70:4631–4644. https://doi.org/10.1007/s00018-013-1411-4
9. Corsten MF, Heggermont W, Papageorgiou A-P, Deckx S, Tijsma A, Verhesen W, van Leeuwen R, Carai P, Thibaut H-J, Custers K, Summer G, Hazebroek M, Verheyen F, Neyts J, Schroen B, Heymans S. 2015. The microRNA-221/-222 cluster balances the antiviral and inflammatory response in viral myocarditis. Eur Heart J 36:2909–2919. https://doi.org/10.1093/eurheartj/ehv321
10. Jiang D, Li M, Yu Y, Shi H, Chen R. 2019. microRNA-34a aggravates Coxsackievirus B3-induced apoptosis of cardiomyocytes through the

SIRT1-p53 pathway. J Med Virol 91:1643–1651. https://doi.org/10.1002/jmv.25482
11. Zhang X, Gao X, Hu J, Xie Y, Zuo Y, Xu H, Zhu S. 2019. ADAR1p150 forms a complex with dicer to promote miRNA-222 activity and regulate PTEN expression in CVB3-induced viral myocarditis. IJMS 20:407. https://doi.org/10.3390/ijms20020407
12. Zhang BY, Zhao Z, Jin Z. 2016. Expression of miR-98 in myocarditis and its influence on transcription of the FAS/FASL gene pair. Genet. Mol. Res 15. https://doi.org/10.4238/gmr.15027627
13. He F, Xiao Z, Yao H, Li S, Feng M, Wang W, Liu Z, Liu Z, Wu J. 2019. The protective role of microRNA-21 against Coxsackievirus B3 infection through targeting the MAP2K3/P38 MAPK signaling pathway. J Transl Med 17:335. https://doi.org/10.1186/s12967-019-2077-y
14. He J, Yue Y, Dong C, Xiong S. 2013. MiR-21 confers resistance against CVB3-induced myocarditis by inhibiting PDCD4-mediated apoptosis. Clin Invest Med 36:E103–11. https://doi.org/10.25011/cim.v36i2.19573
15. Wang L, Qin Y, Tong L, Wu S, Wang Q, Jiao Q, Guo Z, Lin L, Wang R, Zhao W, Zhong Z. 2012. MiR-342-5p suppresses Coxsackievirus B3 biosynthesis by targeting the 2C-coding region. Antiviral Res 93:270–279. https://doi.org/10.1016/j.antiviral.2011.12.004
16. Tong L, Lin L, Wu S, Guo Z, Wang T, Qin Y, Wang R, Zhong X, Wu X, Wang Y, Luan T, Wang Q, Li Y, Chen X, Zhang F, Zhao W, Zhong Z. 2013. MiR-10A* up-regulates Coxsackievirus B3 biosynthesis by targeting the 3D-coding sequence. Nucleic Acids Res. 41:3760–3771. https://doi.org/10.1093/nar/gkt058
17. Trobaugh DW, Gardner CL, Sun C, Haddow AD, Wang E, Chapnik E, Mildner A, Weaver SC, Ryman KD, Klimstra WB. 2014. RNA viruses can hijack vertebrate microRNAs to suppress innate immunity. Nature 506:245–248. https://doi.org/10.1038/nature12869
18. Huang J, Wang F, Argyris E, Chen K, Liang Z, Tian H, Huang W, Squires K, Verlinghieri G, Zhang H. 2007. Cellular microRNAs contribute to HIV-1 latency in resting primary CD4+ T lymphocytes. Nat Med 13:1241–1247. https://doi.org/10.1038/nm1639
19. Dubey SK, Shrinet J, Sunil S. 2019. Aedes aegypti microRNA, miR-2944B-5p interacts with 3'UTR of chikungunya virus and cellular target vps-13 to regulate viral replication. PLoS Negl Trop Dis 13:e0007429. https://doi.org/10.1371/journal.pntd.0007429
20. Jopling CL. 2008. Regulation of hepatitis C virus by microRNA-122. Biochem Soc Trans 36:1220–1223. https://doi.org/10.1042/BST0361220
21. Amador-Cañizares Y, Panigrahi M, Huys A, Kunden RD, Adams HM, Schinold MJ, Wilson JA. 2018. miR-122, small RNA annealing and sequence mutations alter the predicted structure of the hepatitis C virus 5' UTR RNA to stabilize and promote viral RNA accumulation. Nucleic Acids Res 46:9776–9792. https://doi.org/10.1093/nar/gky662
22. Chahal J, Gebert LFR, Gan HH, Camacho E, Gunsalus KC, MacRae IJ, Sagan SM. 2019. miR-122 and ago interactions with the HCV genome alter the structure of the viral 5' terminus. Nucleic Acids Res 47:5307–5324. https://doi.org/10.1093/nar/gkz194
23. Wen W, He Z, Jing Q, Hu Y, Lin C, Zhou R, Wang X, Su Y, Yuan J, Chen Z, Yuan J, Wu J, Li J, Zhu X, Li M. 2015. Cellular microRNA-miR-548g-3p modulates the replication of dengue virus. J Infect 70:631–640. https://doi.org/10.1016/j.jinf.2014.12.001
24. Hsu PW-C, Lin L-Z, Hsu S-D, Hsu JB-K, Huang H-D. 2007. ViTa: prediction of host microRNAs targets on viruses. Nucleic Acids Res 35:D381–5. https://doi.org/10.1093/nar/gkl1009
25. Rennie W, Liu C, Carmack CS, Wolenc A, Kanoria S, Lu J, Long D, Ding Y. 2014. STarMir: a web server for prediction of microRNA binding sites. Nucleic Acids Res 42:W114–8. https://doi.org/10.1093/nar/gku376
26. Liu C, Mallick B, Long D, Rennie WA, Wolenc A, Carmack CS, Ding Y. 2013. CLIP-based prediction of mammalian microRNA binding sites. Nucleic Acids Res 41:e138. https://doi.org/10.1093/nar/gkt435
27. Long D, Lee R, Williams P, Chan CY, Ambros V, Ding Y. 2007. Potent effect of target structure on microRNA function. Nat Struct Mol Biol 14:287–294. https://doi.org/10.1038/nsmb1226
28. Ray PS, Das S. 2002. La autoantigen is required for the internal ribosome entry site-mediated translation of Coxsackievirus B3 RNA. Nucleic Acids Res 30:4500–4508. https://doi.org/10.1093/nar/gkf583
29. Dave P, George B, Sharma DK, Das S. 2017. Polypyrimidine tract-binding protein (PTB) and PTB-associated splicing factor in CVB3 infection: an ITAF for an ITAF. Nucleic Acids Res. 45:9068–9084. https://doi.org/10.1093/nar/gkx519
30. Verma B, Ponnuswamy A, Gnanasundram SV, Das S. 2011. Cryptic AUG is important for 48S ribosomal assembly during internal initiation of translation of Coxsackievirus B3 RNA. J Gen Virol 92:2310–2319. https://doi.org/10.1099/vir.0.032151-0
31. Zhang X, Li Y, Wang D, Wei X. 2017. miR-22 suppresses tumorigenesis and improves radiosensitivity of breast cancer cells by targeting Sirt1. Biol Res 50:27. https://doi.org/10.1186/s40659-017-0133-8
32. Wu H, Liu J, Zhang Y, Li Q, Wang Q, Gu Z. 2021. miR-22 suppresses cell viability and EMT of ovarian cancer cells via NLRP3 and inhibits Pi3K/AKT signaling pathway. Clin Transl Oncol 23:257–264. https://doi.org/10.1007/s12094-020-02413-8
33. Xu D, Takeshita F, Hino Y, Fukunaga S, Kudo Y, Tamaki A, Matsunaga J, Takahashi RU, Takata T, Shimamoto A, Ochiya T, Tahara H. 2011. miR-22 represses cancer progression by inducing cellular Senescence. J Cell Biol 193:409–424. https://doi.org/10.1083/jcb.201010100
34. Fan T, Wang CQ, Li XT, Yang H, Zhou J, Song YJ. 2021. MiR-22-3p suppresses cell migration and invasion by targeting PLAGL2 in breast cancer. J Coll Physicians Surg Pak 31:937–940. https://doi.org/10.29271/jcpsp.2021.08.937
35. Yang QY, Yang KP, Li ZZ. 2020. MiR-22 restrains proliferation of rheumatoid arthritis by targeting IL6R and may be concerned with the suppression of NF-κB pathway. Kaohsiung J Med Sci 36:20–26. https://doi.org/10.1002/kjm2.12124
36. Ji Q, Wang X, Cai J, Du X, Sun H, Zhang N. 2020. MiR-22-3p regulates amyloid β deposit in mice model of alzheimer's disease by targeting mitogen-activated protein kinase 14. CNR 16:473–480. https://doi.org/10.2174/1567202616666191111124516
37. Xia P, Chen J, Liu Y, Cui X, Wang C, Zong S, Wang L, Lu Z. 2022. MicroRNA-22-3p ameliorates alzheimer's disease by targeting SOX9 through the NF-κB signaling pathway in the hippocampus. J Neuroinflammation 19:180. https://doi.org/10.1186/s12974-022-02548-1
38. Huang Z-P, Wang D-Z. 2014. miR-22 in cardiac remodeling and disease. Trends Cardiovasc Med 24:267–272. https://doi.org/10.1016/j.tcm.2014.07.005
39. Huang Z-P, Chen J, Seok HY, Zhang Z, Kataoka M, Hu X, Wang D-Z. 2013. MicroRNA-22 regulates cardiac hypertrophy and remodeling in response to stress. Circ Res 112:1234–1243. https://doi.org/10.1161/CIRCRESAHA.112.300682
40. George B, Dave P, Rani P, Behera P, Das S. 2021. Cellular protein HuR regulates the switching of genomic RNA templates for differential functions during the Coxsackievirus B3 life cycle. J Virol 95:e0091521. https://doi.org/10.1128/JVI.00915-21
41. Liu M, Yang Q, Han J. 2022. Transcriptomic analysis reveals that Coxsackievirus B3 woodruff and GD strains use similar key genes to induce FoxO signaling pathway activation in HeLa cells. Arch Virol 167:131–140. https://doi.org/10.1007/s00705-021-05292-8
42. Yao M, Xu C, Shen H, Liu T, Wang X, Shao C, Shao S. 2020. The regulatory role of miR-107 in Coxsackie B3 virus replication. Aging 12:14467–14479. https://doi.org/10.18632/aging.103488
43. Hanson PJ, Hossain AR, Qiu Y, Zhang HM, Zhao G, Li C, Lin V, Sulaimon S, Vlok M, Fung G, Chen VH, Jan E, McManus BM, Granville DJ, Yang D. 2019. Cleavage and sub-cellular redistribution of nuclear pore protein 98 by Coxsackievirus B3 protease 2A impairs cardioprotection. Front Cell Infect Microbiol 9:265. https://doi.org/10.3389/fcimb.2019.00265
44. Mi H, Thomas P. 2009. PANTHER pathway: an ontology-based pathway database coupled with data analysis tools. Methods Mol Biol 563:123–140. https://doi.org/10.1007/978-1-60761-175-2_7
45. Ye Z, Yang Y, Wei Y, Li L, Wang X, Zhang J. 2022. Pcdh1 promotes progression of pancreatic ductal adenocarcinoma via activation of NF-κB signalling by interacting with KPNB1. Cell Death Dis 13:633. https://doi.org/10.1038/s41419-022-05087-y
46. Jangra RK, Herbert AS, Li R, Jae LT, Kleinfelter LM, Slough MM, Barker SL, Guardado-Calvo P, Román-Sosa G, Dieterle ME, et al. 2018. Protocadherin-1 is essential for cell entry by new world hantaviruses. Nature 563:559–563. https://doi.org/10.1038/s41586-018-0702-1
47. Shi C, Xu X. 2013. MicroRNA-22 is down-regulated in hepatitis B virus-related hepatocellular carcinoma. Biomed Pharmacother 67:375–380. https://doi.org/10.1016/j.biopha.2013.03.002
48. Wang L, Wang Y-S, Mugiyanto E, Chang W-C, Yvonne Wan Y-J. 2020. MiR-22 as a metabolic Silencer and liver tumor suppressor. Liver Res 4:74–80. https://doi.org/10.1016/j.livres.2020.06.001

49. Moheimani F, Koops J, Williams T, Reid AT, Hansbro PM, Wark PA, Knight DA. 2018. Influenza A virus infection dysregulates the expression of microRNA-22 and its targets; CD147 and HDAC4, in epithelium of asthmatics. Respir Res 19:145. https://doi.org/10.1186/s12931-018-0851-7
50. Xiao S, Du T, Wang X, Ni H, Yan Y, Li N, Zhang C, Zhang A, Gao J, Liu H, Pu F, Zhang G, Zhou E-M. 2016. Mir-22 promotes porcine reproductive and respiratory syndrome virus replication by targeting the host factor HO-1. Vet Microbiol 192:226–230. https://doi.org/10.1016/j.vetmic.2016.07.026
51. Morán J, Ramírez-Martínez G, Jiménez-Alvarez L, Cruz A, Pérez-Patrigeon S, Hidalgo A, Orozco L, Martínez A, Padilla-Noriega L, Avila-Moreno F, Cabello C, Granados J, Ortíz-Quintero B, Ramírez-Venegas A, Ruíz-Palacios GM, Zlotnik A, Merino E, Zúñiga J. 2015. Circulating levels of miR-150 are associated with poorer outcomes of A/H1N1 infection. Exp Mol Pathol 99:253–261. https://doi.org/10.1016/j.yexmp.2015.07.001
52. Zhou D, Li Q, Jia F, Zhang L, Wan S, Li Y, Song Y, Chen H, Cao S, Ye J. 2020. The Japanese encephalitis virus NS1′ protein inhibits type I IFN production by targeting MAVS. J Immunol 204:1287–1298. https://doi.org/10.4049/jimmunol.1900946
53. Wan S, Ashraf U, Ye J, Duan X, Zohaib A, Wang W, Chen Z, Zhu B, Li Y, Chen H, Cao S. 2016. MicroRNA-22 negatively regulates poly(I:C)-triggered type I interferon and inflammatory cytokine production via targeting mitochondrial antiviral signaling protein (MAVS). Oncotarget 7:76667–76683. https://doi.org/10.18632/oncotarget.12395
54. Zhao X, Ma X, Guo J, Mi M, Wang K, Zhang C, Tang X, Chang L, Huang Y, Tong D. 2019. Circular RNA CircEZH2 suppresses transmissible gastroenteritis coronavirus-induced opening of mitochondrial permeability transition pore via targeting MiR-22 in IPEC-J2. Int J Biol Sci 15:2051–2064. https://doi.org/10.7150/ijbs.36532
55. Kadmon CS, Landers CT, Li HS, Watowich SS, Rodriguez A, King KY. 2017. MicroRNA-22 controls interferon alpha production and erythroid maturation in response to infectious stress in mice. Exp Hematol 56:7–15. https://doi.org/10.1016/j.exphem.2017.09.001
56. Esfandiarei M, Boroomand S, Suarez A, Si X, Rahmani M, McManus B. 2007. Coxsackievirus B3 activates nuclear factor kappa B transcription factor via a phosphatidylinositol-3 kinase/protein kinase B-dependent pathway to improve host cell viability. Cell Microbiol 9:2358–2371. https://doi.org/10.1111/j.1462-5822.2007.00964.x
57. Wang Y, Sun Z, Zhang H, Song Y, Wang Y, Xu W, Li M. 2023. CVB3 inhibits NLRP3 Inflammasome activation by suppressing NF-κB pathway and ROS production in LPS-induced macrophages. Viruses 15:1078. https://doi.org/10.3390/v15051078
58. Pinkert S, Kopp A, Brückner V, Fechner H, Beling A. 2020. Single-point mutations within the Coxsackie B virus receptor-binding site promote resistance against soluble virus receptor traps. J Virol 94:e00952-20. https://doi.org/10.1128/JVI.00952-20
59. Bopegamage S, Berakova K, Gomocak P, Baksova R, Galama J, Hyoty H, Tauriainen S. 2021. Primary site of Coxsackievirus B replication in the small intestines: no proof of peyer's patches involvement. Microorganisms 9:2600. https://doi.org/10.3390/microorganisms9122600
60. Uhlén M, Fagerberg L, Hallström BM, Lindskog C, Oksvold P, Mardinoglu A, Sivertsson Å, Kampf C, Sjöstedt E, Asplund A, et al. 2015. Proteomics. tissue-based map of the human proteome. Science 347:1260419. https://doi.org/10.1126/science.1260419
61. Yoon JH, Srikantan S, Gorospe M. 2012. MS2-TRAP (MS2-tagged RNA affinity purification): tagging RNA to identify associated miRNAs. Methods 58:81–87. https://doi.org/10.1016/j.ymeth.2012.07.004